Human ADA2 deficiency is characterized by the absence of an intracellular hypoglycosylated form of adenosine deaminase 2

Short title: DADA2 cells lack lysosomal LMW-ADA2

Authors:

Lisa Ehlers[1,2,3,4,5] (ORCID: 0000-0001-8737-001X), Marjon Wouters[1] (ORCID: 0000-0002-4675-1665), Anneleen Hombrouck[1] (ORCID: 0009-0003-5236-6063), Bethany Pillay[1] (ORCID: 0000-0001-7964-544X), Selket Delafontaine[1,6] (ORCID: 0000-0002-8985-8155), Giorgia Bucciol[1,6] (ORCID: 0000-0001-5004-0738), Marco Baggio[1,7] (ORCID: 0000-0001-6708-9925), Mariia Dzhus[1] (ORCID: 0000-0002-2077-4295), Emma Francés Rabanal[1], Alexandra Damerau[5,8] (0000-0001-6651-2963), Julia Neugebauer[9] (ORCID: 0000-0002-2576-1012), Frédéric Ebstein[10] (ORCID: 0000-0002-3729-7878), Maarten Jacquemyn[11] (ORCID: 0000-0003-2626-4189), Lien De Somer[12,13] (ORCID: 0000-0002-8488-5090), Rik Schrijvers[14] (ORCID: 0000-0002-4261-6220), Steven Vanderschueren[15] (ORCID: 0000-0002-4003-5465), David Cassiman[16] (ORCID: 0000-0002-6154-0970), Marieluise Kirchner[17] (ORCID: 0000-0002-7049-534X), Philipp Mertins[17] (ORCID: 0000-0002-2245-528X), Mir-Farzin Mashreghi[4,5], Tilmann Kallinich[2,3,4,5] (ORCID: 0000-0003-2404-9397), Dirk Daelemans[7] (ORCID: 0000-0001-7092-1153), Patrizia Agostinis[18] (ORCID: 0000-0003-1314-2115), Leen Moens[1] (ORCID: 0000-0002-5347-6526), Isabelle Meyts[1] (ORCID: 0000-0003-1214-0302)

Affiliations:

[1] Department of Microbiology, Immunology and Transplantation, Laboratory for Inborn Errors of Immunity, KU Leuven, Leuven, Belgium

[2] Department of Pediatric Respiratory Medicine, Immunology and Critical Care Medicine, Charité – Universitätsmedizin Berlin, corporate member of Freie Universität Berlin and Humboldt-Universität zu Berlin, Berlin, Germany

[3] Berlin Institute of Health at Charité – Universitätsmedizin Berlin, Berlin, Germany

[4] German Center for Child and Adolescent Health (DZKJ), partner site Berlin, Berlin, Germany

[5] Deutsches Rheuma-Forschungszentrum, an Institute of the Leibniz Association, Berlin, Germany

[6] Department of Pediatrics, University Hospitals Leuven, KU Leuven, Leuven, Belgium

[7] Laboratory of Computational and Developmental Biology, Berlin Institute for Medical Systems Biology (BIMSB), Max-Delbrück-Centrum for Molecular Medicine in the Helmholtz Association (MDC), Berlin, Germany

[8] Department of Rheumatology and Clinical Immunology, Charité – Universitätsmedizin Berlin, corporate member of Freie Universität Berlin and Humboldt-Universität zu Berlin, Berlin, Germany

[9] Department of Pediatric Gastroenterology, Nephrology and Metabolic Diseases, Center of Chronically Sick Children, Charité – Universitätsmedizin Berlin, corporate member of Freie Universität Berlin and Humboldt-Universität zu Berlin, Berlin, Germany

[10] Nantes University, CHU Nantes, CNRS, INSERM, Nantes, France

[11] KU Leuven, Department of Microbiology, Immunology and Transplantation, Rega Institute for Medical Research, Molecular Genetics and Therapeutics in Virology and Oncology Research Group, Leuven, Belgium

[12] Department of Pediatric Rheumatology, University Hospitals Leuven, Leuven, Belgium

45 [13] Laboratory of Immunobiology, Department of Microbiology and Immunology, KU Leuven,
46 Leuven, Belgium
47 [14] Department of Microbiology, Immunology and Transplantation, Allergy and Clinical immunology
48 Research group, KU Leuven, Leuven, Belgium
49 [15] Department of General Internal Medicine, Research Department Microbiology, Immunology, and
50 Transplantation, Laboratory of Clinical Infectious and Inflammatory Disorders, University Hospitals
51 Leuven, Leuven, Belgium
52 [16] Department of Gastroenterology-Hepatology and Metabolic Center, University Hospital Leuven,
53 Leuven, Belgium
54 [17] Core Unit Proteomics, Berlin Institute of Health at Charité - Universitätsmedizin Berlin and Max-
55 Delbrück-Center for Molecular Medicine, Berlin, Germany
56 [18] Cell Death Research & Therapy (CDRT) Lab, Department of Cellular & Molecular Medicine, Center
57 for Cancer Biology, VIB-KU Leuven, Leuven, Belgium
58
59 **Corresponding author:**
60 Isabelle Meyts, Laboratory for Inborn Errors of Immunity and Department of Pediatrics UZ Leuven,
61 Herestraat 49, 3000 Leuven, Belgium; Tel +32 16 343841; Fax +32 16 343842;
62 isabelle.meyts@uzleuven.be

Abstract

Human deficiency of adenosine deaminase 2 (DADA2) is an autoinflammatory disease caused by pathogenic variants in *ADA2* that lead to impaired deaminase activity. Recently, a lysosomal function of ADA2 has been proposed but an intracellular form of the protein has not yet been characterized. Here, we analyze protein expression of mutant ADA2 in human monocyte-derived macrophages from 10 DADA2 patients. We identify an intracellular low-molecular-weight (LMW) form of ADA2 that undergoes glycan trimming by α-mannosidases and is absent in DADA2 macrophages. Subcellular fractionation and immunofluorescence microscopy demonstrate that LMW-ADA2 is localized in the lysosomes. By overexpression of 34 *ADA2* variants in HEK293T and U-937 cells, we show that absence of LMW-ADA2 strongly correlates with reduced deaminase activity and predicts variant pathogenicity. In conclusion, we describe a previously unreported intracellular hypoglycosylated form of ADA2 and establish the absence of this LMW-ADA2 as a cellular characteristic of DADA2. Thereby, we introduce a protein correlate of the recently described lysosomal form of ADA2.

Summary

Ehlers et al. demonstrate that mutant ADA2 fails to undergo glycan processing beyond the ER leading to the absence of intracellular low-molecular-weight (LMW) ADA2 in DADA2 patients' macrophages. LMW-ADA2 localizes to the lysosomes and can be generated from extracellular wild-type ADA2.

81 # Introduction

82 Human deficiency of adenosine deaminase 2 (DADA2) is an inborn error of immunity caused by
83 biallelic deleterious mutations in the *ADA2* gene *(1, 2)*. The disease manifests with a diverse phenotype
84 displaying features of both autoinflammation and immunodeficiency *(3)*. More than 600 missense or
85 predicted loss-of-function variants in *ADA2* are listed in the Genome Aggregation Database
86 (gnomAD v4.1.0) *(4)*. In the Infevers registry, 116 *ADA2* variants are classified as (likely) pathogenic
87 *(5)*. Complete loss-of-function variants are more likely to cause bone marrow failure. Missense variants
88 which account for 80% of pathogenic variants are found in patients with a primarily vasculitis
89 phenotype as well as in those presenting with cytopenias and hypogammaglobulinemia *(6, 7)*. Our
90 group recently demonstrated that specific monoallelic *ADA2* variants can cause ADA2 deficiency
91 through a dominant negative mechanism *(8)*.

92 How mutations in *ADA2* give rise to this diverse phenotype, even in patients with identical genotypes,
93 is not understood. Inflammatory symptoms of the disease typically respond well to tumor necrosis
94 factor-alpha inhibitors (TNFi) *(9)*. Insufficient resolution of bone marrow failure in response to this
95 treatment however often necessitates hematopoietic stem cell transplantation and disease lethality still
96 is 8% *(10)*. To develop improved treatment options, we require a better understanding of the
97 pathomechanisms underlying the immunological and clinical phenotype of DADA2.

98 ADA2 is a 59-kD glycoprotein with a signal peptide that mediates secretion of the protein via the
99 endoplasmic reticulum (ER), and exhibits extracellular adenosine deaminase activity as a homodimer
100 *(11)*. The protein has four N-glycosylation sites and insufficient glycosylation leads to ER retention
101 and intracellular aggregate formation of ADA2 transfected into HEK293T cells *(12, 13)*. Impaired
102 protein secretion and absent serum ADA2 enzyme activity have been established as characteristics
103 shared by the majority of pathogenic *ADA2* variants *(14)*. Mechanistic approaches to the
104 pathophysiology of ADA2-deficient cells have therefore been based on impaired extracellular

105 adenosine deamination driving inflammation *(15, 16)*. This assumption fails to acknowledge the weak
106 affinity of ADA2 for adenosine and the presence of functional ADA1 in DADA2 patients *(17)*.
107 Research into alternative functions of the ADA2 protein and DADA2-causing variants is therefore
108 warranted. Biochemical characterization of pathogenic *ADA2* variants has until now mostly been
109 performed in a HEK293T overexpression system with supraphysiological intracellular levels of ADA2
110 while expression of the mutant protein has been shown to be minimal in DADA2 $CD14^+$ monocytes
111 *(14, 18, 19)*. Disease-associated *ADA2* variants have to date hardly been studied in their physiological
112 milieu.
113 In this study, we analyze trafficking and glycosylation of endogenous ADA2 expressed in primary
114 human macrophages from healthy donors and DADA2 patients. We provide evidence of an
115 intracellular glycoform of ADA2 that results from glycan trimming by Golgi α-mannosidases and show
116 that DADA2 macrophages do not express this low-molecular-weight-form of ADA2. Absence of
117 LMW-ADA2 correlates with reduced ADA2 enzyme activity and serves as a biomarker of variant
118 pathogenicity.
119

120 # Results

121 ***In vitro* macrophage differentiation partially restores ADA2 protein expression in DADA2**
122 **monocytes**

123 Of the circulating leukocytes, monocytes express ADA2 most abundantly. We analyzed ADA2 protein
124 expression and *ADA2* mRNA levels in peripheral blood monocytes of 10 DADA2 patients and three
125 heterozygous carriers (**Table 1** and **Fig. S1A+B**). $CD14^+$ monocytes from DADA2 patients showed
126 very low or absent ADA2 protein expression despite normal *ADA2* mRNA levels in patients with
127 missense mutations which account for 80% of pathogenic variants found in DADA2 patients (**Fig. 1A**
128 and **Fig. S2A**). Upon macrophage differentiation, we observed an increase in mutant ADA2 protein

129 expression in the patient cells while ADA2 protein expression was reduced in healthy control (HC)
130 human monocyte-derived macrophages (HMDM) (**Fig. 1B**). Successful differentiation of DADA2
131 HMDM was achieved both with granulocyte–macrophage colony-stimulating factor (GM-CSF) and
132 macrophage colony-stimulating factor (M-CSF) (**Fig. S2B**), which confirms the reported restoration
133 of macrophage differentiation of monocytes from DADA2 patients under treatment with TNFi *(9)*.
134 Interestingly, western blotting of pathogenic ADA2 protein variants expressed in DADA2 HMDM
135 revealed the presence of only a high-molecular-weight (HMW) band of around 60 kD compared to
136 HC HMDM displaying two bands at 60 and 57 kD, with the low-molecular-weight (LMW) band being
137 more pronounced (**Fig. 1B** and **Fig. S2C**). This protein expression pattern of pathogenic *ADA2*
138 variants was confirmed in ADA2$^{-/-}$ U-937 cells transduced with the variants p.G47R, p.G47V and
139 p.R169Q (**Fig. 1C** and **Fig. S2D**). In order to verify our finding in a larger number of *ADA2* variants,
140 we analyzed the protein expression of mutant ADA2 by transfection of HEK293T cells.
141 Overexpression of tagged WT ADA2 and several confirmed pathogenic variants uniformly led to
142 predominant intracellular expression of HMW-ADA2 (63 kD) (**Fig. 1D**). In line with our findings in
143 DADA2 HMDM, intracellular LMW-ADA2 was absent after overexpression of mutant ADA2 in
144 HEK293T cells (**Fig. 1D**). Interestingly, this band was still present – albeit at lower intensity – in the
145 variants p.N127Q and p.W326R, two variants not reported in DADA2 patients but created for the
146 study of ADA2 glycosylation and dimerization, respectively *(11, 12)*. The molecular weight of secreted
147 wild-type (WT) ADA2 in the supernatant of HC HMDM or transfected HEK293T cells corresponded
148 to the intracellular HMW form – the only form expressed in DADA2 HMDM (**Fig. 1B+D**). We
149 confirmed the secretion of HMW-ADA2 in the monocytic cell lines U-937 and THP-1 (**Fig. S2E**).
150 HMDM from DADA2 patient P8 showed residual secretion of HMW-ADA2 with a molecular weight
151 equivalent to secreted WT ADA2 (**Fig. S2F**). This HMW-form of ADA2 also corresponded to the
152 ADA2 form detected in human serum (**Fig. 1E**). Collectively, we show that HC HMDM intracellularly

153 express a form of ADA2 that is lower in molecular weight than the secreted protein. This LMW-form
154 is absent in DADA2 HMDM which only express the HMW-form intracellularly.
155
156 **Human monocyte-derived macrophages intracellularly express a hypoglycosylated low-**
157 **molecular-weight form of ADA2 that is absent in DADA2 macrophages**
158 Differences in the molecular weight of a protein can be caused by posttranslational protein
159 modifications and N-glycosylation of ADA2 has previously been confirmed *(11, 13, 18)*. Therefore,
160 we initially hypothesized that the LMW-form of ADA2 unique to cells expressing WT ADA2
161 corresponded to glycan-free ADA2. To test this, we performed glycan removal on lysates and
162 supernatants containing ADA2 protein (**Fig. 2A**). Complete removal of N-glycans by Peptide-N-
163 Glycosidase F (PNGase F) yielded a difference in molecular weight of 7 kD between HMW-ADA2
164 and glycan-free ADA2 both overexpressed in HEK293T cells and endogenously expressed in the
165 monocytic cell lines U-937 and THP-1 as well as HMDM (**Fig. 2B+C**), revealing that LMW-ADA2
166 was in fact slightly larger than glycan-free ADA2. Importantly, the anti-ADA2 antibody clone
167 EPR25430-131 (#ab288296; abcam) was superior in detecting LMW-ADA2 but poorly detected
168 glycan-free ADA2 (**Fig. S3A**). Glycan removal by PNGase F eliminated the differences in molecular
169 weight between the LMW-form and the HMW-form in HMDM, yielding a single band of glycan-free
170 ADA2 at 53 kD (**Fig. 2C-E**). Hence, the difference in molecular weight between intracellular WT
171 ADA2 (LMW) and secreted WT ADA2 or intracellular pathogenic ADA2 (both HMW) was due to
172 differential protein glycosylation. Of note, glycan removal yielded a smaller band of 53 kD in addition
173 to the glycan-removed 56 kD protein for tagged WT ADA2 overexpressed in HEK293T cells that was
174 absent for all tested pathogenic variants and did not appear after inhibition of N-glycosylation by
175 tunicamycin (**Fig. 2B**). As this band was absent after glycan removal of endogenous WT ADA2, its
176 physiological relevance is unclear.

177 Overall, we showed that the difference in size between HMW- and LMW-ADA2 is due to differential
178 protein glycosylation.
179
180 **N-glycosylated ADA2 undergoes glycan trimming in the ER as part of protein quality control**
181 In order to better characterize the glycosylation of endogenous ADA2, we inhibited N-glycosylation
182 in HMDM and the monocytic cell lines U-937 and THP-1 by 24-hour treatment with tunicamycin. We
183 found that this treatment only acted on the fainter HMW-band while LMW-ADA2 remained
184 unchanged in size (**Fig. 2D+E**). In accordance with previous findings *(13)*, we showed that adenosine
185 deaminase activity of ADA2 was preserved after glycan removal while treatment with tunicamycin
186 reduced enzymatic activity. This was true for ADA2 overexpressed in HEK293T cells as well as
187 endogenous ADA2 from HC HMDM (**Fig. S3B+C**). These findings indicated that N-glycosylation
188 was required for adequate folding of the ADA2 protein. The ER glucosidases I and II form part of
189 the ER quality control by removing glycosyl residues from accurately folded proteins prior to transfer
190 to the Golgi apparatus *(20)*. Treatment with castanospermine, an inhibitor of the ER glucosidases I
191 and II, caused an additional increase in the size of HMW-ADA2 in both HC and DADA2 HMDM
192 (**Fig. 3A**), confirming trimming of N-glycosylated ADA2 in the ER. Since the same shift in molecular
193 weight was observed in DADA2 HMDM, we concluded that processing of WT and mutant does not
194 yet diverge at this early stage of the secretory pathway. As seen previously upon incubation with
195 tunicamycin, the LMW-form of ADA2, which is absent in DADA2 HMDM, was unaffected by this
196 treatment (**Fig. 3A**). We confirmed this finding in the three ADA2-expressing cell lines U-937, THP-
197 1 and Jurkat (**Fig. 3B**). Since hypoglycosylated LMW-ADA2 was still detected after 24-hour treatment
198 with tunicamycin – an inhibitor of the initial step of N-glycosylation – we concluded that glycosylation
199 and trimming of the residual LMW-form must have occurred prior to the initiation of the incubation
200 period, suggesting high stability of LMW-ADA2. Accordingly, LMW-ADA2 was responsive to

201 prolonged incubation with tunicamycin at a lower concentration (**Fig. 3B**). The same was true for
202 inhibition of ER glucosidases: the more stable LMW-ADA2 was unaffected by 24-hour incubation
203 with castanospermine and the detected LMW-form had likely already matured before the beginning of
204 the incubation period. We confirmed the increased stability of LMW-ADA2 compared to HMW-
205 ADA2 by cycloheximide chase assay (**Fig. 3C** and **Fig. S3D**). Besides, this experiment revealed that
206 HMW-ADA2 protein expressed by HEK293T cells transfected with pathogenic *ADA2* variants
207 showed increased intracellular stability compared with the WT protein. This was also true after
208 inhibition of N-glycosylation and after an increased incubation period of 48 hours (**Fig. 3C** and
209 **Fig. S3E**). Since ADA2 is a secreted protein, protein secretion must be taken into account when
210 assessing the intracellular signal reduction in this assay over time (**Fig. S3F**). Impaired secretion has
211 previously been established as a characteristic of pathogenic ADA2 variants *(2, 14)*. We confirmed the
212 secretory defect in HMDM and serum from our DADA2 cohort (**Fig. 3D**). Overexpression in
213 HEK293T cells recapitulated the endogenous behavior of the respective variants well (**Fig. 3D**).
214 Comparing the levels of increased ADA2 stability observed by cycloheximide chase assay with residual
215 protein secretion, the variants p.T129P and p.R169Q that exhibited complete absence of secretion did
216 indeed show the highest levels of intracellular ADA2 24 hours after inhibition of protein synthesis
217 (**Fig. 3C** and **Fig. S3D**). However, intracellular levels of the secreted mutant p.P344L were still higher
218 compared with WT.
219 We next blocked the secretory pathway to impair secretion of WT ADA2 and thereby confirmed that
220 the secretory defect strongly contributed to the increased intracellular protein levels of mutant ADA2
221 (**Fig. 3E** and **Fig. S4**). While the secretory defect of mutant ADA2 was phenocopied by WT ADA2
222 upon incubation with brefeldin A (BFA), we also found that this treatment caused increased
223 degradation of the mutants p.G47V, p.T129P and p.R169Q (**Fig. 3E** and **Fig. S4**). BFA inhibits ER
224 to Golgi trafficking. We observed that treatment of WT ADA2-expressing cells with BFA yielded a

225 single ADA2 band with a molecular weight between that of HMW- and LMW-ADA2 (**Fig. 3B+E**),
226 suggesting that both HMW- and LMW-ADA2 are the result of further glycan processing in the Golgi.
227 Indeed, inhibition of trans Golgi transport by monensin *(21, 22)* did not impair the generation of
228 LMW-ADA2 in cells overexpressing WT ADA2 (**Fig. 3E**). The differential behavior in response to
229 the secretory pathway inhibitors BFA and monensin was confirmed in DADA2 HMDM (**Fig. 3F**).
230 The absence of LMW-ADA2 upon inhibition of ER to Golgi trafficking and the increase in LMW-
231 ADA2 upon inhibition of trans Golgi transport supported our hypothesis that LMW- and HMW-
232 ADA2 are generated from a common precursor glycoform after transport to the Golgi apparatus
233 (**Fig. 3G**).
234 In summary, we showed that N-glycosylation is required for folding and secretion of ADA2 and that
235 both WT and mutant ADA2 are subject to processing by the ER glucosidases I and II while only WT
236 ADA2 undergoes further glycan trimming in the Golgi apparatus.
237
238 **The pathogenic ADA2 variant p.R169Q shows increased binding to proteins of the protein**
239 **folding machinery**
240 After verifying the expression of LMW- and HMW-ADA2 in cells expressing WT ADA2 and an
241 impairment of glycan-processing in DADA2 cells, our aim was to further characterize the different
242 glycoforms of ADA2 in the second part of this study: (i) retained mutant HMW-ADA2, (ii) secreted
243 WT HMW-ADA2 and (iii) intracellular WT LMW-ADA2.
244 First, we performed immunoprecipitation followed by mass spectrometry (IP-MS) to analyze the
245 interactome of WT ADA2 and the pathogenic ADA2 variant p.R169Q transfected into HEK293T
246 cells. p.R169Q displayed increased interaction with proteins involved in the ER quality control
247 machinery for glycoproteins (**Fig. 4A** and **Table S1**). Upon inhibition of N-glycosylation by
248 tunicamycin, we observed a similar increase also for the WT protein (**Fig. 4A** and **Table S1**),

249 highlighting the importance of adequate N-glycosylation for successful folding and secretion of ADA2.
250 Additionally, we observed an increase in lysosomal proteins in the ADA2 interactome after treatment
251 with tunicamycin, suggesting autophagic degradation of non-glycosylated ADA2. Among the induced
252 interactors were several proteins of the chaperone-mediated autophagy pathway, e.g. LAMP2 and
253 HSPA13, and we verified the presence of a KFERQ-related motif (QKFVE, amino acids 274-278) in
254 the sequence of ADA2 *(23)*. IP-MS of HC and DADA2 HMDM did not yield any specific binders,
255 which was possibly due to low protein abundance in the pull down of endogenous ADA2 (**Fig. S5A**).
256 Notably, IP preferentially pulled down the HMW-form of ADA2 (**Fig. S5B+C**). The experiment
257 consequently did not allow us to draw conclusions about the interactome and potential distinctive
258 function of LMW-ADA2.
259 Given the increased binding of mutant ADA2 to the ER folding machinery, we verified whether
260 pathogenic *ADA2* variants induced an increased ER stress response. In line with previous reports *(14)*,
261 we observed that some pathogenic *ADA2* variants caused signs of activation of an ER stress response,
262 measured by increased levels of CHOP (*DDIT3*) and BiP (*HSPA5*) (**Fig. S5D**). These differences
263 were however no longer present after down-titrating the amount of transfected DNA to achieve near-
264 physiological protein levels (**Fig. 4B** and **Fig. S5E+F**) and neither was there a difference in BiP
265 expression in $CD14^+$ monocytes from DADA2 patients compared to healthy controls (**Fig. 4C** and
266 **Fig. S6**). In line with other studies *(8, 24)*, we showed that protein misfolding led to intracellular
267 aggregate formation of mutant ADA2 (**Figure 4D+E**). In summary, our experiments revealed the
268 interaction of the ADA2 variant p.R169Q overexpressed in HEK293T cells with mediators of the
269 folding machinery and ER quality control despite lack of increased ER stress in the presence of
270 pathogenic ADA2 variants. The interactome analyses were inconclusive regarding the characterization
271 of LMW-ADA2.
272

273 **Wild-type HMW-ADA2 is subject to additional glycan maturation prior to secretion**

274 Next, we aimed to further explore the glycan structure of HMW-ADA2. We hypothesized that the ER
275 retention of most pathogenic protein variants of ADA2 leads to incomplete glycan processing. To
276 examine the glycosylation pattern of WT and mutant ADA2, we performed additional glycan removal
277 experiments in ADA2$^{-/-}$ U-937 cells transduced pathogenic *ADA2* variants. We chose a monocytic
278 cell line for these experiments to minimize errors due to differential expression of glycosylation
279 enzymes in different cell types.

280 First, we confirmed that complete N-glycan removal by PNGase F cancelled out the differences in
281 molecular weight between HMW- and LMW-ADA2, confirming that they are due to N-glycosylation
282 (**Fig. 5A**). Endo H is another endoglycosidase that cleaves high mannose glycans and – unlike PNGase
283 F – does not remove complex glycans. We found that WT and mutant ADA2 were both sensitive to
284 glycan removal by Endo H (**Fig. 5A+B**), hinting at the presence of high mannose oligosaccharides in
285 both LMW- and HMW-ADA2 glycans. In contrast with PNGase F treatment, glycan removal by Endo
286 H revealed differences between WT and mutant ADA2: Compared with mutant ADA2, Endo H-
287 treated WT ADA2 visualized as a smear on western blot as opposed to the clean single band observed
288 for mutant ADA2 in U-937 cells and HMDM (**Fig. 5A+B**). This suggests that WT ADA2 undergoes
289 additional glycan processing as complex glycans are less sensitive to Endo H. Since the size of LMW-
290 ADA2 makes the presence of additional carbohydrate residues unlikely, we concluded that in WT
291 ADA2-expressing cells, the glycan trees of HMW-ADA2 mature into complex glycans, generating
292 HMW(c)-ADA2, the HMW-form observed in HC HMDM (**Fig. 5C**). For all tested pathogenic
293 variants, glycan removal by Endo H yielded a clean band very close in molecular weight to complete
294 removal of N-glycans by PNGase F (**Fig. 5A**). Consequently, mutant HMW-ADA2 is likely not subject
295 to any glycan maturation beyond the ER, which is in agreement with the postulated ER retention of
296 pathogenic ADA2 protein variants. This finding also implies that WT HMW(c)-ADA2 and mutant

297 HMW-ADA2 – while very similar in molecular weight –differ in their glycan structures and do not
298 represent the same ADA2 glycoform.
299 Collectively, our findings suggest that the N-glycan structures of ADA2 contain high-mannose
300 oligosaccharides and that WT HMW(c)-ADA2 contains complex glycan branches while mutant
301 HMW-ADA2 does not undergo advanced glycan maturation.
302
303 **LMW-ADA2 is generated by glycan trimming through alpha-mannosidases**
304 The addition of complex glycan structures is usually preceded by the removal of α-linked mannose
305 residues in the late ER and Golgi by a set of α-mannosidases *(25)*. We therefore hypothesized that
306 mutant ADA2 is inaccessible to glycan-trimming by endogenous α-mannosidases, accounting for the
307 absence of complex glycan structures as well as the absence of LMW-ADA2. To test this hypothesis,
308 we incubated WT and mutant ADA2-expressing U-937 cells with different inhibitors of glycan-
309 processing enzymes. The corresponding western blots were performed in a capillary-based separation
310 and detection system to allow for a more precise distinction of the different molecular weight peaks.
311 After synthesis and N-glycan transfer in the ER, proteins are initially trimmed by the ER α-glucosidases
312 I and II that are inhibited by castanospermine *(20)*. As shown in HMDM, castanospermine caused an
313 increase in the molecular weight of HMW-ADA2 (**Fig. S7**). By increasing the incubation time
314 ≥ 48 hours we observed a shift also for LMW-ADA2, confirming the superior stability of LMW-
315 ADA2. The change in molecular weight of both HMW- and LMW-ADA2 upon inhibition of the ER
316 α-glucosidases I and II supported our hypothesis that the processing of the two glycoforms only
317 diverges after exiting the ER. After passing the quality control mechanisms in the ER, proteins can be
318 trimmed further by different α-mannosidases in the ER and Golgi. Kifunensine inhibits class I α-
319 mannosidases that are typically found in the late ER and cis-Golgi and cleave α-1,2-linked mannose
320 residues *(20)*. Incubation of U-937 cells with kifunensine led to an increase in the molecular weight of

321 LMW-ADA2 (**Fig. 6A** and **Fig. S7**). After 96 hours, LMW-ADA2 almost overlay HMW-ADA2
322 (**Fig. 6A**). Concomitant incubation with swainsonine led to similar results. However, incubation with
323 swainsonine alone also increased the molecular weight of LMW-ADA2, suggesting that multiple
324 mannosidases are involved in the trimming of LMW-ADA2. Swainsonine inhibits both α-mannosidase
325 II in the medial Golgi and the lysosomal α-mannosidase *(26)*. To better understand whether also the
326 lysosomal enzyme is involved in the trimming of LMW-ADA2, we analyzed HMDM from a patient
327 with α-mannosidosis, harbouring biallelic mutations in *MAN2B1* encoding the lysosomal α-
328 mannosidase *(27)*. We found that the patient's cells phenocopied HC cells treated with the class II α-
329 mannosidase inhibitor swainsonine and that swainsonine treatment did not have an additional effect
330 on the molecular weight of LMW-ADA2 expressed in the lysosomal α-mannosidase-deficient cells
331 (**Fig. 6B**). This finding suggests that LMW-ADA2 undergoes processing not only in the ER and Golgi
332 but also in the lysosomes. Finally, as a proof of principle, we performed glycan removal by α1-2,3,6
333 mannosidase on WT ADA2. This experiment yielded a single band slightly lower but very close in
334 molecular weight to LMW-ADA2 (**Fig. 6C**). This is in line with the findings of the previous
335 experiments since the inhibited glycan-processing enzymes typically do not cleave α-1,6-linked
336 mannose residues, which accounts for the lower molecular weight of α1-2,3,6 mannosidase-treated
337 ADA2 compared with LMW-ADA2 (**Fig. 6D+E**). Importantly, the glycan structures of LMW-ADA2
338 predicted by this set of experiments corresponded with the glycan profile determined in another study
339 (**Fig. S8A**) *(28)*.
340 In summary, we demonstrated that LMW-ADA2 is generated from HMW-ADA2 by glycan-
341 processing through multiple α-mannosidases in the ER, Golgi and lysosomal compartments.
342
343 **LMW-ADA2 localizes to the lysosomes and can be generated from WT HMW(c)-ADA2 in**
344 **ADA2-deficient cells**

345 To further support the processing of LMW-ADA2 by the lysosomal α-mannosidase, we next aimed to
346 verify the lysosomal localization of the LMW-glycoform in monocytic cells. To this end, we performed
347 immunofluorescence microscopy of U-937 cells expressing WT ADA2 or the pathogenic ADA2
348 variant p.R169Q. In cells expressing the WT protein, ADA2 colocalized with the lysosomal marker
349 LAMP1 (**Fig. 7A** and **Fig. S8B**). Moreover, the experiment confirmed ER retention of the mutant
350 protein while WT ADA2 was found in the ER, Golgi and lysosomal compartments (**Fig. 7A**). To
351 verify that the intracellular glycoform of ADA2 localizing to the lysosomes was indeed LMW-ADA2,
352 we then performed subcellular fractionation experiments. We showed that the lysosomal fraction
353 contained only LMW-ADA2 (**Fig. 7B**). LMW-ADA2 was also present in the cytosolic and membrane
354 fractions. HMW-ADA2 localized exclusively to the membranous fraction that also contains ER and
355 Golgi membrane proteins (**Fig. 7B**).
356 Besides intracellular transport, proteins can also enter the lysosomes via the endocytotic pathway. To
357 evaluate whether this route allowed the uptake and processing of ADA2 from the extracellular space,
358 we incubated ADA2$^{-/-}$ U-937 cells with the supernatant of transfected HEK293T cells containing WT
359 HMW(c)-ADA2. We first confirmed that exogenous HMW(c)-ADA2 protein was taken up by the
360 ADA2-deficient cells (**Fig. 7C**). Next, we analyzed whether HMW(c)-ADA2 underwent intracellular
361 glycan processing after uptake. Within the first 6 hours of incubation, HMW-ADA2 was the only
362 glycoform found intracellularly (**Fig. 7D**). After 24 hours, we observed a strong signal for LMW-
363 ADA2 in the whole cell lysate of the ADA2-deficient cells suggesting that exogenous HMW(c)-ADA2
364 was subject to intracellular glycan trimming after uptake (**Fig. 7D**). In accordance with our previous
365 findings, LMW-ADA2 was not found in the supernatant of the incubated cells. This finding also
366 mechanistically adds to our previous observation that LMW-ADA2 exhibits increased stability:
367 Generation of LMW-ADA2 from internalized previously secreted extracellular HMW(c)-ADA2

368 represents an additional mechanism accounting for the prolonged presence of intracellular LMW-
369 ADA2 after inhibition of protein synthesis or N-glycosylation.
370 Finally, we confirmed that the secreted pathogenic *ADA2* variant p.G47A was also taken up into the
371 monocytic cells. Unlike the WT protein, the mutant protein was however not processed into LMW-
372 ADA2 (**Fig. 7D**). These experiments confirm that LMW-ADA2 can be generated from exogenous
373 extracellular ADA2 and that ADA2-deficient cells possess the glycan-processing machinery to generate
374 LMW-ADA2 from the WT protein (**Fig. 7E**).
375
376 **Absence of LMW-ADA2 correlates with impaired ADA2 enzyme activity and predicts the**
377 **pathogenicity of *ADA2* variants**
378 After characterizing LMW-ADA2 as the intracellular glycoform of ADA2 and establishing its absence
379 as a feature of DADA2 cells, we validated our findings on a larger set of *ADA2* variants. For this, we
380 analyzed a total of 34 *ADA2* variants, including 18 variants found in homozygous state in DADA2
381 patients and two variants predicted to be benign with homozygous individuals documented in the
382 gnomAD database (p.H335R and p. R230Q) (gnomAD v4.1.0, https://gnomad.broadinstitute.org).
383 Our data set also included all the *ADA2* variants previously described as DADA2-associated despite
384 an ADA2 enzyme activity above 25% of WT ADA2 *(29)*. The included variants cover all the domains
385 of the ADA2 protein (**Fig. 8A**). The variants were overexpressed in HEK293T cells and studied for
386 LMW-ADA2 expression, ADA2 protein secretion and both extracellular and intracellular ADA2
387 enzyme activity (**Fig. 8B**). In line with our studies on the trafficking of LMW-ADA2, this glycoform
388 was exclusively processed from variants that also showed residual ADA2 secretion (**Fig. 8B**). The
389 greatest part of the pathogenic variants with residual secretion lacking enzymatic activity was also
390 characterized by the absence of LMW-ADA2 (**Fig. 8B**). Overall, we found an excellent correlation
391 between the expression of LMW-ADA2 and extracellular ($r = 0.91$, $p < 0.0001$) or intracellular ADA2

392 enzyme activity ($r = 0.89$, $p < 0.0001$) (**Fig. 8C**). Two pathogenic variants lacking ADA2 enzyme
393 activity – p.H112Q and p.T360A – showed moderate expression of LMW-ADA2. By contrast,
394 p.P334L was characterized by absent LMW-ADA2 and a residual ADA2 enzyme activity > 25%
395 (**Fig. 8C**). All the DADA2-associated variants previously reported to show comparatively high
396 enzymatic activity also showed intermediate levels of LMW-ADA2. Four of those variants were
397 reported in homozygous state in DADA2 patients (**Table 2**). Several of the variants were classified as
398 benign by different pathogenicity scores despite having been reported in DADA2 patients (**Table 2**).
399 Overall, the REVEL, CADD and PolyPhen scores correlated best with pathogenicity by lack of LMW-
400 ADA2 (**Fig. 8D** and **Table S2+3**). SIFT classified the majority of variants as pathogenic despite
401 preserved LMW-ADA2 expression and enzymatic activity while with alpha missense even many clearly
402 pathogenic variants were categorized as benign.
403 In summary, we confirmed that LMW-ADA2 expression of ADA2 protein variants strongly correlates
404 with their adenosine deaminase activity and verified absence of LMW-ADA2 as a robust indicator of
405 pathogenicity.
406

407 # Discussion

408 In this study, we showed that pathogenic protein variants of ADA2 expressed in HMDM from
409 DADA2 patients do not undergo glycan processing beyond the ER and that DADA2 HMDM
410 therefore lack lysosomal LMW-ADA2 and secreted HMW(c)-ADA2. We reported that the LMW-
411 form represents an intracellular glycoform of ADA2 that is generated by α-mannosidase-mediated
412 glycan cleavage after transport to the Golgi apparatus.
413 The importance of N-glycosylation in the trafficking and function of ADA2 has previously been
414 established *(12, 13)*. Yet, the behavior of mutant ADA2 at the cellular level has to date only been
415 examined in overexpression systems of cells that do not express the protein endogenously *(13, 14, 24)*.

416 Importantly, expression of glycosyltransferases and glycosidases and therefore glycosylation patterns
417 of individual proteins show striking variation even between different immune cell populations *(30)*. It
418 is therefore essential to understand the behavior of ADA2 in the patients' primary cells. In our cohort
419 of 10 DADA2 patients, we identified the intracellular predominance of unprocessed HMW-ADA2 in
420 the absence of LMW-ADA2 as a feature that was shared by all missense variants, independently of the
421 patients' clinical phenotype. Differential patterns of glycosylation of the same protein being associated
422 with distinctive protein functions have previously been described: IL-24 is a signal peptide-containing
423 glycoprotein that is secreted via the ER. A partially glycosylated cytosolic form of IL-24 has been
424 shown to mediate protein kinase R activation independently of its extracellular function *(31)*. The
425 predominance of the partially glycan-trimmed LMW-form of ADA2 in HC HMDM raises the question
426 of whether, in a similar way, this form differs in function from secreted HMW(c)-ADA2. In fact, the
427 function of ADA2 has repeatedly been subject to discussion for several reasons: (i.) Pathogenic ADA2
428 variants display a wide spectrum of residual adenosine deaminase function which does not clearly
429 correlate with disease severity *(29)*. (ii.) ADA2 has evolved towards lower affinity to adenosine in higher
430 species *(11)*. (iii.) ADA1 exhibits superior adenosine deaminase activity (Km of 20-50 μM vs. 2-3 mM
431 for ADA2) and extracellular ADA1 bound to CD26 theoretically compensates for the absence of
432 ADA2 at physiological levels of adenosine *(17)*. Yet, the majority of studies proposing possible
433 pathomechanisms underlying the immunological phenotype of DADA2 rely on the role of ADA2 as
434 an extracellular adenosine deaminase *(15, 16)*. In contrast, two groups introduced the possibility of an
435 intracellular function of ADA2 as a lysosomal protein *(28, 32)*. Greiner-Tollersrud and colleagues
436 characterized the glycan structures of ADA2 isolated from porcine brain and identified a high
437 mannose-6-phosphate content, indicating targeting of ADA2 to the lysosome. Indeed, they showed
438 an overlap between the glycosylation pattern of ADA2 with several known lysosomal proteins *(28)*.
439 We showed that the glycan structures of LMW- and HMW-ADA2 expressed in HMDM were sensitive

440 to glycan removal by Endo H, suggesting the presence of high-mannose oligosaccharides *(33)*. This is
441 in line with a potential lysosomal localization of ADA2 that we also confirmed by imaging. Moreover,
442 we showed that multiple – also lysosomal – α-mannosidases are involved in the processing of LMW-
443 ADA2. Combined inhibition of class I and II α-mannosidases caused an increase in the molecular
444 weight of LMW-ADA2 yielding a glycoform almost identical to HMW-ADA2. The current lack of an
445 antibody that sufficiently pulls down the LMW-glycoform by immunoprecipitation prevents a
446 thorough glycan and interactome analysis of LMW-ADA2 at this point in time. We were however able
447 to show that the predicted glycan structures derived from our inhibition experiments aligned perfectly
448 with glycan analyses performed on porcine ADA2 (**Fig. S8A**) *(28)*. Combined with the previous studies
449 *(28, 32)*, our data provide a strong hint that LMW-ADA2 represents the lysosomal glycoform of ADA2
450 and might be functionally distinct from secreted HMW(c)-ADA2. In addition, we show for the first
451 time that exogenous WT ADA2 can be taken up by ADA2-deficient cells and – even more importantly
452 – processed into the intracellular LMW-glycoform (**Fig. 7C+D**). This finding is crucial from a clinical
453 perspective given current endeavors to develop new therapeutic approaches including the use of
454 PEGylated ADA2. Our study provides the first hint at the capacity of externally applied ADA2 to
455 successfully carry out also intracellular functions of ADA2.
456 In the HEK293T model system, transfected ADA2 was predominantly expressed as the HMW-form
457 corresponding to secreted ADA2 in these cells, highlighting the limitations of this system to
458 understand the behavior of endogenous ADA2. Discrepancies between the two systems are also
459 evident from the fact that ADA2 in whole cell lysates from transfected HEK293T cells was equally
460 sensitive to glycan removal by PNGase F or Endo H *(13)*, while we observed some residual glycan
461 structures upon Endo H treatment of ADA2 in lysates from U-937 cells and HMDM (**Fig. 5A+B**).
462 A caveat regarding the relevance of macrophage LMW-ADA2 in the pathogenesis of DADA2 is that
463 in primary $CD14^+$ monocytes, the cells with the highest endogenous expression of ADA2, differentially

464 glycosylated forms of ADA2 cannot be clearly distinguished (**Fig. 1A+B**). Moreover, patient
465 monocytes – both from patients with missense variants with normal *ADA2* mRNA expression and
466 from patients with variants that exhibit nonsense-mediated mRNA decay – show complete absence of
467 mutant ADA2 protein expression. This implies that mutations in the *ADA2* gene might manifest
468 differently on a cellular level depending on the expressing cell.
469 This notion needs to be taken into account when examining the potential induction of ER stress by
470 pathogenic variants of ADA2. Intracellular retention of ADA2 has only been reported after
471 overexpression in HEK293T cells *(2, 14)*. While primary monocytic cells also show impaired secretion
472 of mutant ADA2, intracellular protein levels are very low in HMDM and close to absent in $CD14^+$
473 monocytes. In our cohort of DADA2 patients, we did not observe an increased ER stress response in
474 $CD14^+$ monocytes. This was in line with single-cell RNA-sequencing data reported by Watanabe et al.
475 that showed downregulation of eIF2 signaling – a main pathway of the integrated stress response *(34,*
476 *35)*.
477 Although we could not confirm that the presence of misfolded mutant ADA2 contributes to the
478 pathophysiology of the disease by induction of an unfolded protein response, our data highlight the
479 need for a better understanding of the folding and trafficking mechanisms of WT and mutant ADA2.
480 We verified that the presence of pathogenic ADA2 protein variants as well as inhibition of N-
481 glycosylation provoked the formation of intracellular protein aggregates, thereby extending previous
482 reports *(13, 24)*.
483 Next to Sanger sequencing of the *ADA2* gene, the measurement of serum ADA2 enzyme activity
484 currently represents the diagnostic gold standard for DADA2. Assuming an intracellular function of
485 the protein, it is possible that this strategy may overlook a proportion of patients. In this article, we
486 validated the absence of LMW-ADA2 as a new characteristic of pathogenic *ADA2* variants. We
487 showed that the pathogenic variant p.P344L exhibited complete absence of LMW-ADA2 despite a

488 residual enzyme activity above 25% of WT ADA2. This highlights the potential benefit of additionally
489 checking new variants for LMW-ADA2 expression in the validation process, especially when enzyme
490 activity is inconclusive. Overall, we did however find an excellent correlation between LMW-ADA2
491 expression and enzyme activity, emphasizing that in most cases pathogenic variants affect both glycan
492 processing and catalytic activity. This is in line with a similar correlation shown by Greiner-Tollersrud
493 and colleagues in the study of the lysosomal function of ADA2 *(28)*. It is important to note that both
494 ADA2 enzyme activity and LMW-ADA2 expression are imperfect biomarkers of pathogenicity. We
495 identified 11 DADA2-associated variants with comparatively high LMW-ADA2 expression and
496 enzyme activity (**Table 2**). Described in patients with a DADA2-phenotype, they have all been
497 classified as likely disease-causing. However, given our incomplete understanding of the
498 pathophysiology of DADA2, the pathogenicity of these variants has to be considered uncertain. For
499 p.F355L, Nihira et al. concluded from their analyses that this variant may not be pathogenic, also
500 considering its high allele frequency. Moreover, for ambiguous variants only found in compound
501 heterozygous state in DADA2 patients, dominant-negative effects of the other pathogenic variant also
502 need to be taken into account *(8)*. Lastly, it has to be pointed out that for the variant p.H91R that
503 exhibits close-to-normal enzymatic activity and LMW-ADA2 expression when expressed in HEK293T
504 cells, a homozygous patient has been described that showed strongly reduced serum ADA2 enzyme
505 activity *(36)*. In our study, we showed that – unlike HEK293T cells – $CD14^+$ monocytes expressing
506 pathogenic *ADA2* variants show absent ADA2 expression. Therefore, it is conceivable that the
507 phenotype of certain *ADA2* variants only becomes apparent in the patients' primary cells.
508 Until now, monocytes as the main producers of endogenous ADA2 have received the most attention
509 in deciphering the pathophysiology of the disease. Considering the role of glycosylation in protein
510 folding and the potential impact of this modification on protein function, we cannot exclude that the
511 main ADA2 function might vary even between different immune cells. This might also account for

512 the diverse clinical phenotype of the disease and the varying involvement of different immune cell
513 populations. The large number of pathogenic variants and their diversity with respect to biochemical
514 characteristics are additional factors contributing to the difficulties in delineating a single all-
515 encompassing pathomechanism that explains the complexity of the disease.
516 In conclusion, we demonstrate for the first time the differential N-glycosylation of pathogenic ADA2
517 in patient-derived macrophages. We establish LMW-ADA2 as a hypoglycosylated non-secreted form
518 of ADA2 in healthy controls. This LMW-ADA2 is generated by α-mannosidases after transfer to the
519 Golgi and is absent in DADA2. Further studies will be needed to confirm the functional relevance of
520 these results in the pathogenesis of the disease.
521

522 # Materials and Methods

523 **Experimental design**

524 This exploratory study included patients treated at University Hospitals Leuven and their parents were
525 included as heterozygous carriers. The diagnosis of DADA2 was made based on the clinical phenotype
526 followed by a combination of serum ADA2 enzyme activity and sequencing of the *ADA2* gene
527 according to the DADA2 management guidelines *(37)*. Healthy donors were recruited at University
528 Hospitals Leuven and KU Leuven. This study was approved by the Ethics Committee for Research of
529 Leuven University Hospitals (project numbers S63077, S63807). The patient with α-mannosidosis was
530 recruited at Charité University Hospital in Berlin. The inclusion of the patient from Berlin was
531 approved by the Ethics Committee of Charité University Medicine Berlin (project number
532 EA2/1178/22). The patients provided written informed consent prior to participation. The study was
533 performed in accordance with the ethical standards as laid down in the 1964 Declaration of Helsinki
534 and its later amendments. Our study examined male and female individuals, and similar findings are
535 reported for both sexes.

536 The aim of this study was to determine the protein characteristics of ADA2 endogenously expressed
537 in human immune cells carrying pathogenic *ADA2* variants. To compensate for the limited sample
538 size in the study of patients with rare diseases, our results were validated in two separate *in vitro* models
539 of ADA2 deficiency examining a total of 34 pathogenic *ADA2* variants. The results were confirmed
540 using two different anti-ADA2 antibodies both validated with the help of ADA2 knockout samples
541 and reproduced in two technically distinct blotting systems to exclude technical artefacts.
542
543 **Sanger sequencing**
544 Genomic DNA samples were prepared from heparinized peripheral blood following the instructions
545 of the QIAamp DNA Blood Mini kit (#51104; QIAGEN). Primers were designed with the help of
546 Oligo Primer Analysis Software version 7 (Molecular Biology Insights). ADA2-specific gDNA
547 amplification was performed using Platinum™ SuperFi™ PCR Master Mix (#12358010; Thermo
548 Fisher Scientific). PCR products were purified using the QIAquick PCR purification kit (#28106;
549 QIAGEN). Sanger sequencing was performed on an ABI 3730 XL Genetic Analyzer (Applied
550 Biosystems) at LGC Genomics (Berlin, Germany). Sequencing data were analyzed using Chromas 2.6.5
551 (http://www.technelysium.com.au).
552
553 **Cell culture**
554 Peripheral blood mononuclear cells (PBMCs) were isolated by density gradient centrifugation using
555 Lymphoprep™ (#1114546; PROGEN) in SepMate™ isolation tubes (#85450; STEMCELL
556 Technologies) according to the manufacturer's instructions. Prior to monocyte isolation, the final
557 centrifugation step was performed at 300*xg* for 10 minutes at 4 °C. $CD14^+$ monocytes were isolated
558 magnetically by positive selection using human CD14 MicroBeads (#130-050-201; Miltenyi Biotec) on
559 LS columns (#130-042-401; Miltenyi Biotec) according to the manufacturer's protocol. The cells were

560 eluted into complete medium (RPMI 1640 medium (#61870044; Gibco) supplemented with 10% fetal
561 calf serum (FCS) (#S181BH-500, Biowest) and 1% penicillin-streptomycin (#15140122; Gibco).
562 Purity > 97% of $CD14^+$ monocytes after magnetic sorting was verified by flow cytometry (anti-CD14-
563 FITC clone MφP9, 1:40, #345784; BD Biosciences). For macrophage differentiation, $3x10^5$ $CD14^+$
564 monocytes were seeded in a 12-well plate in 1 mL complete medium containing 20 ng/mL GM-CSF
565 (#300-03; Peprotech) or 50 ng/mL M-CSF (#300-25; Peprotech). The cells were differentiated for ten
566 days, with medium changes every three days. U-937, THP-1 and Jurkat cells (all purchased from
567 ATCC) were cultured in complete RPMI medium. HEK293T cells (ATCC) were cultured in DMEM
568 supplemented with 10% FCS and 1% penicillin-streptomycin. For transfection, the cells were seeded
569 in medium containing no antibiotics.
570 Inhibition of the secretory pathway was achieved by 24-hour incubation with 1 μg/mL brefeldin A
571 (#00-4506-51; Thermo Fisher Scientific) or 2 μg/mL monensin (GolgiStop™, #554724, BD
572 Biosciences). For analysis of N-glycosylation and glycan trimming, the cells were incubated with
573 tunicamycin (#T7765; Sigma-Aldrich) at 2.5 μg/mL (HEK293T cells) or 5 μg/mL (HMDM) and
574 castanospermine (#BML-S107-0100; Enzo Life Sciences) at 100 μg/mL for 24h or 48h. α-
575 mannosidases were inhibited by 72-96h incubation with 375 nM kifunensine (#K1140; Sigma-Aldrich)
576 and/or 10 μM swainsonine (#S8195; Sigma-Aldrich). Monocytes were treated with 1 μg/mL
577 tunicamycin for 24h for ER stress induction.
578
579 **Transfection**
580 The plasmid expressing myc-DDK-tagged wild-type ADA2 (transcript variant 3, NM_001282225) was
581 purchased from OriGene Technologies (#RC238645). Pathogenic *ADA2* variants were created by
582 site-directed mutagenesis using the Q5® Site-Directed Mutagenesis Kit (#E0554; New England
583 Biolabs) according to the manufacturer's instructions. Stable competent E. coli (#C3040H, New

584 England Biolabs) were transformed with the generated constructs. Plasmid DNA was purified with
585 the help of the QIAprep Spin Miniprep Kit (#27104, QIAGEN). Successful mutagenesis was verified
586 by Sanger sequencing (LGC Genomics). HEK293T cells were seeded at $5x10^4$ cells/well in 1 mL in a
587 24-well plate or $2.5x10^5$ cells/well in 2 mL in a 6-well plate 24h prior to transfection. The cells were
588 transfected with 5 ng and 25 ng plasmid DNA, respectively, using Lipofectamine™ 2000 Transfection
589 Reagent (#11668019; Invitrogen) according to the manufacturer's instructions. The medium was
590 changed after 24h. Cells and supernatants were collected 48h after transfection. For the reuptake
591 experiments, HEK293T cells were transfected with 1 μg plasmid expressing untagged wild-type ADA2
592 or tagged wild-type and mutant as indicated. Supernatants were collected after 48 hours and transferred
593 to U-937 cells for a 6-24-hour incubation period.
594
595 **Generation of ADA2$^{-/-}$ cell lines by CRISPR/Cas9**
596 Single-guide RNAs targeting ADA2 from the human CRISPR Brunello library (#73179; addgene) *(38)*
597 were cloned into the lentiCRISPRv2 puro plasmid. lentiCRISPRv2 puro was a gift from Brett Stringer
598 (plasmid #98290; addgene; http://n2t.net/addgene:98290; RRID: Addgene_98290). U-937 cells were
599 transfected by electroporation using the Neon™ Transfection System (#MPK5000; Thermo Fisher
600 Scientific) according to the manufacturer's instructions: $2x10^5$ cells were resuspended in Resuspension
601 Buffer R and mixed with 1 μg plasmid DNA. Electroporation was achieved with the following
602 conditions: 1325V, 10ms, 3 pulses. After electroporation, the cells were directly transferred into 500 μL
603 prewarmed complete RPMI 1640 medium. On day 1 after transfection, puromycin (#ant-pr-1;
604 InvivoGen) was added at a final concentration of 1 μg/mL. After 36h, cells were seeded at 1 cell/well
605 in 100 μL RPMI 1640 medium supplemented with 20% FCS in a round bottom 96-well plate. After
606 14 days, the clones were screened for knock out of ADA2 by western blot.
607

608 **Transduction**

609 Pathogenic *ADA2* variants were created by site-directed mutagenesis as described above. Fragments
610 containing the sequence coding for the untagged ADA2 protein were then generated using the
611 following primers and CloneAmp™ HiFi PCR Premix (#639298; Takara Bio):
612 ORF_ADA2_PSPXI_F_GGTGGTACTCGAGTATGTTGGTGGATGGCCCATCTGA;
613 ORF_ADA2_PmeI_R_GGTGGTGTTTAAACCTTTGTAGCCACATCTGCTATGAACTT.
614 The fragments were cleaned up using the QIAquick PCR Purification Kit (#28104; QIAGEN) and
615 cloned into the p3D lentiviral expression vector as follows: Restriction of the expression vector was
616 performed in CutSmart buffer (#B7204; New England Biolabs) with PspX1 (#R0656; New England
617 Biolabs) and PmeI (#R0560; New England Biolabs) at 37 °C overnight followed by 20-minute heat
618 inactivation at 65 °C. Dephosphorylation of 5´-ends was performed using rSAP (#M0371; New
619 England Biolabs) at 37 °C overnight followed by 20-minute heat inactivation at 65 °C. The PCR
620 fragments were subsequently inserted into the expression vector using T4 ligase (#M0202; New
621 England Biolabs) for 10 minutes at room temperature followed by 10-minute heat inactivation at
622 65 °C. After DNA cleanup (#28104; QIAGEN), stable competent E. coli (#C3040H, New England
623 Biolabs) were transformed with the generated plasmids. Plasmid DNA was purified with the help of
624 the QIAprep Spin Miniprep Kit (#27104, QIAGEN). Sanger sequencing (LGC Genomics) was
625 performed to confirm that the genetic information for ADA2 was intact and that the respective
626 mutations were present. Lentiviral particles were generated by transfecting HEK293T cells with the
627 plasmids p3A (Gag-Pol), p3B (Rev), p3C (VSV-G) and p3D (expression vector) at a ratio of 1:1:1:3
628 using Lipofectamine™ 2000 Transfection Reagent (#11668019; Invitrogen). Supernatants containing
629 lentiviral particles were harvested 48h and 72h after transfection. The viral titer was determined using
630 the qPCR Lentivirus Titer Kit (#LV900; Applied Biological Materials). Viral supernatants were
631 prepared at MOI=40 with 8 μg/mL polybrene and 10^6 U-937 cells were transduced by spinoculation

632 at 700*xg* for 2 hours at 32 °C. After 4 hours at 37 °C, the supernatant was replaced by fresh complete
633 RPMI medium. Selection with 1 μg/mL puromycin (#ant-pr-1; InvivoGen) was started 48 hours after
634 the transduction.
635
636 **Subcellular fractionation**
637 Membrane and cytosolic fractions were generated from $10x10^6$ U-937 cells using the Mem-PER™
638 Plus Membrane Protein Extraction Kit (#89842; Thermo Fisher Scientific). Incubation times were
639 optimized to increase protein yield to 45 minutes for the permeabilization buffer and 90 minutes for
640 the solubilization buffer. The lysosomal fraction was produced with the help of the Lysosome
641 Enrichment Kit for Tissues and Cultured Cells (#89839; Thermo Fisher Scientific) according to the
642 manufacturer's protocol.
643
644 **Glycan removal**
645 Glycan removal was performed on whole cell lysates generated with NP-40 lysis buffer or precipitated
646 supernatant protein reconstituted in NP-40 lysis buffer. Glycan removal was performed on 20 μg,
647 10 μg or 25 μg total protein using PNGase F (#P0704; New England Biolabs), Endo H (#P0702; New
648 England Biolabs), α1-2,3,6 Mannosidase (#P0768; New England Biolabs) or PNGase F (#A39245;
649 Gibco) according to the manufacturer's instructions. Glycan removal with PNGase F (#P0704; New
650 England Biolabs) was completed under denaturing conditions for 1 h at 37 °C or under non-
651 denaturing conditions for 4 h at 37 °C as indicated.
652
653 **Immunoblotting**
654 Adherent cells were detached with trypsin-EDTA (0.05%) (#25300062; Gibco) for 5 minutes at 37 °C
655 and the reaction was blocked by addition of complete medium. Cells were pelleted by centrifugation

656 at 400*xg* for 5 minutes at 4 °C. Whole cell lysates were obtained by lysing $1x10^6$ cells in 25 μL RIPA
657 buffer (150 mM NaCl, 1% Triton X-100, 0.5% sodium deoxycholate, 0.1% SDS, pH 8.0) or NP-40
658 lysis buffer (150 mM NaCl, 50 mM Tris-HCl, 1% NP-40, pH 7.4) containing protease inhibitor
659 (#78429; Thermo Fisher Scientific) for 30 minutes on ice, followed by centrifugation at 13,500*xg* for
660 20 minutes at 4 °C.
661 To collect supernatants, cells were cultured in serum-free medium for 24 h. For immunoblotting,
662 supernatants were concentrated by adding 1200 μL ice-cold acetone to 300 μL supernatant and
663 overnight storage at -20°C. Supernatant proteins were then precipitated by centrifugation at 15,000*xg*
664 for 15 minutes at 4°C. The protein pellet was resuspended in 25 μL NP-40 buffer containing protease
665 inhibitor. Bolt™ LDS sample buffer (#B0007; Thermo Fisher Scientific) mixed with Bolt™ Sample
666 Reducing Agent (#B0009; Thermo Fisher Scientific) was added to the samples prior to gel
667 electrophoresis. For analysis of intracellular dimer formation, the reducing agent was omitted. Samples
668 were heated for 5 minutes at 70 °C. Supernatants from HEK293T cells transfected with ADA2 were
669 diluted 1:10 in 2X Bolt™ LDS sample buffer (#B0007; Thermo Fisher Scientific), serum was diluted
670 1:200. SeeBlue™ Plus2 Pre-stained Protein Standard (#LC5925; Thermo Fisher Scientific) was used
671 as protein molecular weight marker.
672 Proteins were transferred onto PVDF transfer membranes. The membranes were probed with the
673 following primary antibodies: anti-ADA2 (clone EPR25430-131, #ab288296, 1:1000; abcam), anti-
674 ADA2 (#HPA007888, 1:500; Sigma-Aldrich; RRID: AB_1078495), Clone OTI4C5, anti-DDK
675 (FLAG) (clone OTI4C5, #TA50011, 1:1000; OriGene Technologies; RRID: AB_2622345), anti-BiP
676 (#3183, 1:1000; Cell Signaling; RRID: AB_10695864), anti-LAMP-1 (clone H4A3, #sc-20011; 1:500;
677 Santa Cruz Biotechnology; RRID: AB_626853), anti-CD98 (clone E-5, #sc-376815, 1:500; Santa Cruz
678 Biotechnology; RRID: AB_2938854), anti-GAPDH (clone 7B, #sc-69778, 1:500; Santa Cruz
679 Biotechnology; RRID: AB_1124759), anti-β-actin (clone: AC-15, #A5441, 1:9,000; Sigma-Aldrich;

680 RRID: AB_476744) at 4°C overnight or at room temperature for two hours. The membranes were
681 washed and incubated with the respective HRP-coupled secondary antibodies for one hour at room
682 temperature: goat anti-rabbit IgG H&L (#ab205718, 1:5000; abcam; RRID: AB_2819160), goat anti-
683 mouse IgG (H + L) (#71045, 1:5000; Sigma-Aldrich; RRID: AB_11211441) or VeriBlot Detection
684 Reagent (#ab131366, 1:1000 in tris saline/5% skim milk; abcam).
685 The anti-ADA2 antibody (clone EPR25430-131, #ab288296, 1:1000; abcam) was used in the following
686 figures of the article: 1A, 1B, 1C, 1D, 1E, 3A, 3B, 3C (left), 3D, 3E, 3F, 4D, 4E, 5B (right), 6A, 6B, 6C
687 (top), 7C, 7D, S2C, S2D, S2E, S2F, S3A, S3D, S3F, S4, S5C, S5E, S5F, S6 and S7. The anti-ADA2
688 antibody (#HPA007888, 1:500; Sigma-Aldrich; RRID: AB_1078495) was applied in the remaining
689 blots: 2B, 2C, 2D, 2E, 3C (right), 5A, 5B (left), 6C (bottom), 7B, S3B, S3C, S3E, S5B.
690 Protein expression was visualized by enzymatic chemiluminescence using Pierce™ ECL western
691 blotting substrate (#32106; Thermo Fisher Scientific) or SuperSignal™ West Pico PLUS
692 Chemiluminescent Substrate (#34580; Thermo Fisher Scientific) in a ChemiDoc XRS+ Imaging
693 System (Bio-Rad).
694 The experiments examining the glycan-processing of LMW-ADA2 were performed in a Wes
695 Automated Western Blot System (ProteinSimple / bio-techne) according to the manufacturer's
696 instructions. Samples were loaded at a final protein concentration of 0.4 mg/mL.
697
698 **Immunoprecipitation**
699 Whole cell lysates were prepared from HEK293T cells transfected with wild-type *ADA2* or the variant
700 p.R169Q or HMDM from HC or DADA2 patients in NP-40 lysis buffer at a protein concentration of
701 1 mg/mL. Primary antibodies were added to 1000 µg lysate or 500 µg lysate, respectively, and
702 incubated rotating at 4 °C overnight. Alternatively, 1 mL supernatant was directly incubated with the
703 primary antibodies. After overexpression, tagged ADA2 was pulled down using 1 µg anti-DDK

704 (FLAG) clone OTI4C5 (#TA50011, OriGene Technologies). An isotype control sample was
705 incubated with 1 μg mouse IgG1 (#02-6100; Invitrogen) in parallel. Endogenous ADA2 was pulled
706 down using 1 μg anti-ADA2 (clone EPR25430-131, #ab288296, abcam) with rabbit monoclonal IgG
707 (clone EPR25A, #ab172730; abcam) used as isotype control. For immunoprecipitation, the samples
708 were rotated with 100 μL SureBeads™ Protein G Magnetic Beads (#1614023, Bio-Rad) for 1h at room
709 temperature. The beads were magnetized and washed four times with PBS/0.1% Tween 20. Samples
710 for mass spectrometric analysis were washed twice with NP-40 lysis buffer and twice with PBS. For
711 western blot, the samples were eluted from the beads in Bolt™ LDS sample buffer (#B0007; Thermo
712 Fisher Scientific).
713
714 **Protein digest**
715 Beads from immunoprecipitation experiments were resuspended in 20 μL denaturation buffer (6 M
716 Urea, 2 M Thiourea, 10 mM HEPES, pH 8.0), reduced for 30 minutes at 25 °C in 12 mM
717 dithiothreitol, followed by alkylation with 40 mM chloroacetamide for 20 minutes at 25 °C. Samples
718 were first digested with 0.5 μg endopeptidase LysC (Wako, Osaka, Japan) for 4 h. After diluting the
719 samples with 80 μL 50 mM ammonium bicarbonate (pH 8.5), 1 μg sequence grade trypsin (Promega)
720 was added overnight at 25 °C. The peptide-containing supernatant was collected and acidified with
721 formic acid (1% final concentration) to stop the digestion. Peptides were desalted and cleaned up using
722 Stage Tip protocol *(39)*. After elution with 80% acetonitrile/0.1% formic acid, samples were dried
723 using speedvac, resolved in 3% acetonitrile/0.1% formic acid and analyzed by LC-MS/MS.
724
725 **LC-MS/MS analyses**
726 Peptides were separated on a reversed-phase column (20 cm fritless silica microcolumns with an inner
727 diameter of 75 μm, packed with ReproSil-Pur C18-AQ 3 μm resin (Dr. Maisch GmbH) using a 90-

728 minute gradient with a 250 nL/min flow rate of increasing Buffer B concentration (from 2% to 60%)
729 on a High-Performance Liquid Chromatography (HPLC) system (Thermo Fisher Scientific) and
730 ionized using an electrospray ionization (ESI) source (Thermo Fisher Scientific) and analyzed on a
731 Thermo Q Exactive HF-X instrument (HEK293T) or on an Q Exactive Plus instrument (HMDM).
732 The Q Exactive HF-X instrument was run in data dependent mode selecting the top 20 most intense
733 ions in the MS full scans, selecting ions from 350 to 2000 m/z, using 60 K resolution with a $3x10^6$ ion
734 count target and 10 ms injection time. Tandem MS was performed at a resolution of 15 K. The MS2
735 ion count target was set to $1x10^5$ with a maximum injection time of 100 ms. Only precursors with
736 charge state 2–6 were selected for MS2. The dynamic exclusion duration was set to 30 s with a 10-ppm
737 tolerance around the selected precursor and its isotopes. The Q Exactive Plus instrument was run in
738 data dependent mode selecting the top 10 most intense ions in the MS full scans, selecting ions from
739 350 to 2000 m/z, using 70 K resolution with a $3x10^6$ ion count target and 50 ms injection time. Tandem
740 MS was performed at a resolution of 17.5 K. The MS2 ion count target was set to $5x10^4$ with a
741 maximum injection time of 250 ms. Only precursors with charge state 2–6 were selected for MS2. The
742 dynamic exclusion duration was set to 30 s with a 10-ppm tolerance around the selected precursor and
743 its isotopes.
744 Raw data were analyzed using MaxQuant software package (v1.6.3.4) *(40)*. The internal Andromeda
745 search engine was used to search MS2 spectra against a human UniProt database (HUMAN.2020-06),
746 including ADA2 mutant sequence, containing forward and reverse sequences. The search included
747 variable modifications of methionine oxidation, N-terminal acetylation and fixed modification of
748 carbamidomethyl cysteine. The FDR was set to 1% for peptide and protein identifications. Unique
749 and razor peptides were considered for quantification. The LFQ (label-free quantitation) algorithm
750 was activated. The resulting text file was filtered to exclude reverse database hits, potential
751 contaminants, and proteins only identified by site.

752

753 **Microscopy**

754 HMDM were differentiated with GM-CSF or M-CSF for 10 days in a 12-well plate as described above.
755 Cell morphology was evaluated in the culture plate by brightfield microscopy on an EVOS M7000
756 Microscope Imaging System (#AMF7000; Invitrogen) using the 20X objective.

757 The immunofluorescence staining was performed in V-shaped 96-well plates in the dark at room
758 temperature (RT). Cells were harvested, fixed in 4% (v/v) paraformaldehyde (Electron Microscopy
759 Sciences) for 10 minutes, and permeabilized with PBS containing 0.1% Tween®20 (Qbiogene Inc.)
760 for 10 minutes. To prevent nonspecific antibody binding, cells were incubated in blocking buffer (1x
761 PBS supplemented with 5% FCS and 5 mg/mL human IgG; IgG1 66.6%, IgG2 28.5%, IgG3 2.7%,
762 IgG4 2.2%; Grifols) for 30 minutes.

763 For the primary staining, an unconjugated rabbit anti-ADA2 antibody (clone EPR25430-131,
764 #ab288296, 1:100; abcam) was applied, followed by incubation with a secondary antibody (donkey
765 anti-rabbit AF488, 1:500, #A-21206, Invitrogen or goat anti-rabbit AF546, 1:500, #A-11035,
766 Invitrogen). In addition, co-staining was performed using rabbit anti-GM130 AF647 (clone D6B1,
767 1:100, #59890, Cell Signaling Technology) in combination with either rabbit anti-LAMP1 AF488
768 (clone D2D11, 1:100, #58996, Cell Signaling Technology) or rabbit anti-calnexin AF555 (clone C5C9,
769 1:100, #23198, Cell Signaling Technology). All antibodies were diluted in 1X PBS supplemented with
770 5% FCS, 5 mg/mL human IgG, and 0.1% Tween®20, and incubated for 2 hours at RT. After each
771 incubation step, cells were washed three times with PBS. Nuclear staining was performed as the final
772 step using DAPI (1 μg/mL in PBS / 0.1% Tween®20) for 15 minutes. For imaging, stained cells were
773 transferred onto glass slides using a Cytospin 4 centrifuge (Thermo Fisher Scientific) at 800 rpm for 3
774 minutes with medium acceleration. Images were acquired with a laser scanning confocal fluorescence
775 microscope (LSM 710, Carl Zeiss).

776

777 **ADA2 enzyme activity**

778 Adenosine deaminase 2 enzyme activity was determined in whole cell lysates from HEK293T cells
779 overexpressing ADA2 or HMDM with and without glycan removal as well as in supernatants from
780 transfected HEK293T cells and human serum. Deaminase activity was measured in a colorimetric
781 assay adapted from Giusti and Galanti *(41)*. Erythro-9-(2-hydroxy-3-nonyl) adenine (EHNA) (#E114;
782 Sigma-Aldrich) was used to inhibit ADA1 activity. Triplicate measurements were performed for all
783 samples. Enzymatic activity of pathogenic ADA2 variants overexpressed HEK293T cells was
784 normalized to the activity of wild-type ADA2.

785

786 **qPCR**

787 5-10x10^5 cells were lysed in TRIzol™ Reagent (#15596018; Thermo Fisher Scientific) for 3 minutes
788 at room temperature and homogenized before storage at -80 °C. To measure the ER stress response,
789 HEK293T cells were seeded at 5x10^4 cells/ml in a 24-well plate 24 h prior to transfection. TRIzol™
790 samples were prepared 48h after transfection. RNA was extracted using the PureLink™ RNA Mini
791 Kit (#12183018A; Thermo Fisher Scientific) according to the manufacturer's instruction. cDNA was
792 generated from 20 ng RNA using the SuperScript™ VILO™ cDNA Synthesis Kit (#11754050;
793 Thermo Fisher Scientific). Quantitative polymerase chain reaction (qPCR) analysis was performed with
794 SsoAdvanced™ Universal SYBR® Green Supermix (#1725271; Bio-Rad Laboratories) and the
795 following primers:

796 ADA2(929-1038)_F_GGCTCCGAATCAAGTTCCCC;

797 ADA2(929-1038)_R_TAAGGCAGCTTAACGCCATCC;

798 ADA2(1138-1257)_F_ACCAGAATCGGCCATGGA;

799 ADA2(1138-1257)_R_CTACAGGGTGGTTCCTCAAGTCA;

800 HSPA5_F_CAAGCAACCAAAGACGCTGGA; HSPA5_R_GCCACCCAGGTCAAACACCA;
801 DDIT3_F_AGAGGAAGAATCAAAAATCT; DDIT3_R_AGCTCTGACTGGAATCTGGA;
802 GAPDH_F_GTCTCCTCTGACTTCAACAGCG;
803 GAPDH_R_ACCACCCTGTTGCTGTAGCCAA.
804 For all conditions, three technical replicates were measured. The experiment was run on a
805 QuantStudio™ 3 Real-Time PCR System (Thermo Fisher Scientific) and analyzed using the
806 QuantStudio™ Design & Analysis Software v1.5.2. The relative abundance of *ADA2* was normalized
807 to the expression level of *GAPDH*. and different conditions were compared using the $2^{-\Delta\Delta Ct}$ method
808 *(42)*.
809
810 **Statistical analysis**
811 Statistical analysis was performed in R using the packages stats and Hmisc. Correlation was measured
812 using Pearson's correlation coefficient.
813 Statistical analysis of the mass spectrometry data was performed using Perseus software (v1.6.2.1) *(43)*.
814 Log2 transformed LFQ intensity values were filtered for minimum of 3 valid values in at least one
815 experimental group and missing values were imputed with random low intensity values taken from a
816 normal distribution. Differences in protein abundance between groups were calculated using two-
817 sample Student's t-test using an FDR-based significance cut-off of 5% (*HEK293T*) or 10% (*HMDM*)
818 in order to define enriched proteins.
819

820 # References

821 1. Q. Zhou, D. Yang, A. K. Ombrello, A. V. Zavialov, C. Toro, A. V. Zavialov, D. L. Stone, J. J.
822 Chae, S. D. Rosenzweig, K. Bishop, K. S. Barron, H. S. Kuehn, P. Hoffmann, A. Negro, W. L.
823 Tsai, E. W. Cowen, W. Pei, J. D. Milner, C. Silvin, T. Heller, D. T. Chin, N. J. Patronas, J. S. Barber,

824 C.-C. R. Lee, G. M. Wood, A. Ling, S. J. Kelly, D. E. Kleiner, J. C. Mullikin, N. J. Ganson, H. H.
825 Kong, S. Hambleton, F. Candotti, M. M. Quezado, K. R. Calvo, H. Alao, B. K. Barham, A. Jones,
826 J. F. Meschia, B. B. Worrall, S. E. Kasner, S. S. Rich, R. Goldbach-Mansky, M. Abinun, E. Chalom,
827 A. C. Gotte, M. Punaro, V. Pascual, J. W. Verbsky, T. R. Torgerson, N. G. Singer, T. R. Gershon,
828 S. Ozen, O. Karadag, T. A. Fleisher, E. F. Remmers, S. M. Burgess, S. L. Moir, M. Gadina, R.
829 Sood, M. S. Hershfield, M. Boehm, D. L. Kastner, I. Aksentijevich, Early-onset stroke and
830 vasculopathy associated with mutations in ADA2. *N. Engl. J. Med.* **370**, 911–920 (2014).
831 2. P. Navon Elkan, S. B. Pierce, R. Segel, T. Walsh, J. Barash, S. Padeh, A. Zlotogorski, Y. Berkun, J.
832 J. Press, M. Mukamel, I. Voth, P. J. Hashkes, L. Harel, V. Hoffer, E. Ling, F. Yalcinkaya, O.
833 Kasapcopur, M. K. Lee, R. E. Klevit, P. Renbaum, A. Weinberg-Shukron, E. F. Sener, B.
834 Schormair, S. Zeligson, D. Marek-Yagel, T. M. Strom, M. Shohat, A. Singer, A. Rubinow, E. Pras,
835 J. Winkelmann, M. Tekin, Y. Anikster, M.-C. King, E. Levy-Lahad, Mutant adenosine deaminase
836 2 in a polyarteritis nodosa vasculopathy. *N. Engl. J. Med.* **370**, 921–931 (2014).
837 3. I. Meyts, I. Aksentijevich, Deficiency of Adenosine Deaminase 2 (DADA2): Updates on the
838 Phenotype, Genetics, Pathogenesis, and Treatment. *J. Clin. Immunol.* **38**, 569–578 (2018).
839 4. K. J. Karczewski, L. C. Francioli, G. Tiao, B. B. Cummings, J. Alföldi, Q. Wang, R. L. Collins, K.
840 M. Laricchia, A. Ganna, D. P. Birnbaum, L. D. Gauthier, H. Brand, M. Solomonson, N. A. Watts,
841 D. Rhodes, M. Singer-Berk, E. M. England, E. G. Seaby, J. A. Kosmicki, R. K. Walters, K.
842 Tashman, Y. Farjoun, E. Banks, T. Poterba, A. Wang, C. Seed, N. Whiffin, J. X. Chong, K. E.
843 Samocha, E. Pierce-Hoffman, Z. Zappala, A. H. O'Donnell-Luria, E. V. Minikel, B. Weisburd, M.
844 Lek, J. S. Ware, C. Vittal, I. M. Armean, L. Bergelson, K. Cibulskis, K. M. Connolly, M.
845 Covarrubias, S. Donnelly, S. Ferriera, S. Gabriel, J. Gentry, N. Gupta, T. Jeandet, D. Kaplan, C.
846 Llanwarne, R. Munshi, S. Novod, N. Petrillo, D. Roazen, V. Ruano-Rubio, A. Saltzman, M.
847 Schleicher, J. Soto, K. Tibbetts, C. Tolonen, G. Wade, M. E. Talkowski, B. M. Neale, M. J. Daly,

848 D. G. MacArthur, The mutational constraint spectrum quantified from variation in 141,456
849 humans. *Nature* **581**, 434–443 (2020).
850 5. Infevers: an online database for autoinflammatory mutations. Copyright. Available at
851 https://infevers.umai-montpellier.fr/ Accessed 14/08/2023. (available at https://infevers.umai-
852 montpellier.fr/web/instructions_for_use.php).
853 6. P. Y. Lee, E. S. Kellner, Y. Huang, E. Furutani, Z. Huang, W. Bainter, M. F. Alosaimi, K. Stafstrom,
854 C. D. Platt, T. Stauber, S. Raz, I. Tirosh, A. Weiss, M. B. Jordan, C. Krupski, D. Eleftheriou, P.
855 Brogan, A. Sobh, Z. Baz, G. Lefranc, C. Irani, S. S. Kilic, R. El-Owaidy, M. R. Lokeshwar, P.
856 Pimpale, R. Khubchandani, E. P. Chambers, J. Chou, R. S. Geha, P. A. Nigrovic, Q. Zhou,
857 Genotype and functional correlates of disease phenotype in deficiency of adenosine deaminase 2
858 (DADA2). *J. Allergy Clin. Immunol.* **145**, 1664-1672.e10 (2020).
859 7. M. Dzhus, L. Ehlers, M. Wouters, K. Jansen, R. Schrijvers, L. De Somer, S. Vanderschueren, M.
860 Baggio, L. Moens, B. Verhaaren, R. Lories, G. Bucciol, I. Meyts, A Narrative Review of the
861 Neurological Manifestations of Human Adenosine Deaminase 2 Deficiency. *J. Clin. Immunol.*
862 (2023), doi:10.1007/s10875-023-01555-y.
863 8. M. Wouters, L. Ehlers, W. Van Eynde, M. E. Kars, S. Delafontaine, V. Kienapfel, M. Dzhus, R.
864 Schrijvers, P. De Haes, S. Struyf, G. Bucciol, Y. Itan, A. Bolze, A. Voet, A. Hombrouck, L. Moens,
865 B. Ogunjimi, I. Meyts, Dominant negative ADA2 mutations cause ADA2 deficiency in
866 heterozygous carriers. *J. Exp. Med.* **222**, e20250499 (2025).
867 9. N. T. Deuitch, D. Yang, P. Y. Lee, X. Yu, N. S. Moura, O. Schnappauf, A. K. Ombrello, D. Stone,
868 H. S. Kuehn, S. D. Rosenzweig, P. Hoffmann, C. Cudrici, D. M. Levy, E. Kessler, J. B. Soep, A.
869 D. Hay, A. Dalrymple, Y. Zhang, L. Sun, Q. Zhang, X. Tang, Y. Wu, K. Rao, H. Li, H. Luo, Y.
870 Zhang, J. M. Burnham, M. Boehm, K. Barron, D. L. Kastner, I. Aksentijevich, Q. Zhou, TNF

871 inhibition in vasculitis management in adenosine deaminase 2 deficiency (DADA2). *J. Allergy Clin.*
872 *Immunol.* **149**, 1812-1816.e6 (2022).
873 10. H. Hashem, A. R. Kumar, I. Müller, F. Babor, R. Bredius, J. Dalal, A. P. Hsu, S. M. Holland, D.
874 D. Hickstein, S. Jolles, R. Krance, G. Sasa, M. Taskinen, M. Koskenvuo, J. Saarela, J. van
875 Montfrans, K. Wilson, B. Bosch, L. Moens, M. Hershfield, I. Meyts, Hematopoietic stem cell
876 transplantation rescues the hematological, immunological, and vascular phenotype in DADA2.
877 *Blood* **130**, 2682–2688 (2017).
878 11. A. V. Zavialov, X. Yu, D. Spillmann, G. Lauvau, A. V. Zavialov, Structural basis for the growth
879 factor activity of human adenosine deaminase ADA2. *J. Biol. Chem.* **285**, 12367–12377 (2010).
880 12. P. Y. Lee, Y. Huang, Q. Zhou, O. Schnappauf, M. S. Hershfield, Y. Li, N. J. Ganson, N. Sampaio
881 Moura, O. M. Delmonte, S. S. Stone, M. J. Rivkin, S.-Y. Pai, T. Lyons, R. P. Sundel, V. W. Hsu, L.
882 D. Notarangelo, I. Aksentijevich, P. A. Nigrovic, Disrupted N-linked glycosylation as a disease
883 mechanism in deficiency of ADA2. *J. Allergy Clin. Immunol.* **142**, 1363-1365.e8 (2018).
884 13. M. Ito, Y. Maejima, K. Nishimura, Y. Nakae, A. Ono, S. Iwaki-Egawa, A role for N-glycosylation
885 in active adenosine deaminase 2 production. *Biochim. Biophys. Acta BBA - Gen. Subj.* **1866**, 130237
886 (2022).
887 14. L. Chen, A. Mamutova, A. Kozlova, E. Latysheva, F. Evgeny, T. Latysheva, K. Savostyanov, A.
888 Pushkov, I. Zhanin, E. Raykina, M. Kurnikova, I. Mersiyanova, C. D. Platt, H. Jee, K. Brodeur, Y.
889 Du, M. Liu, A. Weiss, G. S. Schulert, J. Rodriguez-Smith, M. S. Hershfield, I. Aksentijevich, Q.
890 Zhou, P. A. Nigrovic, A. Shcherbina, E. Alexeeva, P. Y. Lee, Comparison of disease phenotypes
891 and mechanistic insight on causal variants in patients with DADA2. *J. Allergy Clin. Immunol.* (2023),
892 doi:10.1016/j.jaci.2023.04.014.
893 15. C. Carmona-Rivera, S. S. Khaznadar, K. W. Shwin, J. A. Irizarry-Caro, L. J. O'Neil, Y. Liu, K. A.
894 Jacobson, A. K. Ombrello, D. L. Stone, W. L. Tsai, D. L. Kastner, I. Aksentijevich, M. J. Kaplan,

895 P. C. Grayson, Deficiency of adenosine deaminase 2 triggers adenosine-mediated NETosis and
896 TNF production in patients with DADA2. *Blood* **134**, 395–406 (2019).
897 16. R. Dhanwani, M. Takahashi, I. T. Mathews, C. Lenzi, A. Romanov, J. D. Watrous, B. Pieters, C.
898 C. Hedrick, C. A. Benedict, J. Linden, R. Nilsson, M. Jain, S. Sharma, Cellular sensing of
899 extracellular purine nucleosides triggers an innate IFN-β response. *Sci. Adv.* **6**, eaba3688 (2020).
900 17. T. K. Tarrant, S. J. Kelly, M. S. Hershfield, Elucidating the pathogenesis of adenosine deaminase
901 2 deficiency: current status and unmet needs. *Expert Opin. Orphan Drugs* **9**, 257–264 (2021).
902 18. O. K. Greiner-Tollersrud, V. Boehler, E. Bartok, M. Krausz, A. Polyzou, J. Schepp, M. Seidl, J. O.
903 Olsen, C. R. Smulski, S. Raieli, K. Hübscher, E. Trompouki, R. Link, H. Ebersbach, H. Srinivas,
904 M. Marchant, D. Staab, D. Guerini, S. Baasch, P. Henneke, G. Kochs, G. Hartmann, R. Geiger, B.
905 Grimbacher, M. Warncke, M. Proietti, *ADA2 is a lysosomal DNase regulating the type-I interferon response*
906 (2020; https://www.biorxiv.org/content/10.1101/2020.06.21.162990v2), p. 2020.06.21.162990.
907 19. L. Ehlers, M. Wouters, B. Pillay, S. Delafontaine, M. Dzhus, M. Baggio, T. Niehues, G. Dückers,
908 L. Sevenants, K. Casteels, L. D. Somer, R. Schrijvers, S. Vanderschueren, M. Jacquemyn, D.
909 Daelemans, A. Hombrouck, E. P. Chambers, T. Tousseyn, G. Bucciol, P. Agostinis, L. Moens, I.
910 Meyts, Inhibition of lysosomal degradation increases expression of mutant ADA2 in DADA2
911 monocytes. *J. Allergy Clin. Immunol.* **0** (2025), doi:10.1016/j.jaci.2025.06.009.
912 20. A. Varki, R. D. Cummings, J. D. Esko, P. Stanley, G. W. Hart, M. Aebi, D. Mohnen, T. Kinoshita,
913 N. H. Packer, J. H. Prestegard, R. L. Schnaar, P. H. Seeberger, Eds., *Essentials of Glycobiology* (Cold
914 Spring Harbor Laboratory Press, Cold Spring Harbor (NY), ed. 4th, 2022;
915 http://www.ncbi.nlm.nih.gov/books/NBK579918/).
916 21. T. Fujiwara, K. Oda, S. Yokota, A. Takatsuki, Y. Ikehara, Brefeldin A causes disassembly of the
917 Golgi complex and accumulation of secretory proteins in the endoplasmic reticulum. *J. Biol. Chem.*
918 **263**, 18545–18552 (1988).

919 22. H. H. Mollenhauer, D. James Morré, L. D. Rowe, Alteration of intracellular traffic by monensin;
920 mechanism, specificity and relationship to toxicity. *Biochim. Biophys. Acta BBA - Rev. Biomembr.* **1031**,
921 225–246 (1990).
922 23. P. Kirchner, M. Bourdenx, J. Madrigal-Matute, S. Tiano, A. Diaz, B. A. Bartholdy, B. Will, A. M.
923 Cuervo, Proteome-wide analysis of chaperone-mediated autophagy targeting motifs. *PLOS Biol.*
924 **17**, e3000301 (2019).
925 24. S. M. Bowers, M. Sundqvist, P. Dancey, D. A. Cabral, K. L. Brown, Pathogenic variant c.1052T>A
926 (p.Leu351Gln) in adenosine deaminase 2 impairs secretion and elevates type I IFN responsive gene
927 expression. *Front. Immunol.* **13** (2022) (available at
928 https://www.frontiersin.org/articles/10.3389/fimmu.2022.995191).
929 25. K. Legler, R. Rosprim, T. Karius, K. Eylmann, M. Rossberg, R. M. Wirtz, V. Müller, I. Witzel, B.
930 Schmalfeldt, K. Milde-Langosch, L. Oliveira-Ferrer, Reduced mannosidase MAN1A1 expression
931 leads to aberrant N-glycosylation and impaired survival in breast cancer. *Br. J. Cancer* **118**, 847–856
932 (2018).
933 26. D. R. Rose, Structure, mechanism and inhibition of Golgi α-mannosidase II. *Curr. Opin. Struct. Biol.*
934 **22**, 558–562 (2012).
935 27. D. Malm, Ø. Nilssen, Alpha-mannosidosis. *Orphanet J. Rare Dis.* **3**, 21 (2008).
936 28. O. K. Greiner-Tollersrud, M. Krausz, V. Boehler, A. Polyzou, M. Seidl, A. Spahiu, Z. Abdullah,
937 K. Andryka-Cegielski, F. I. Dominick, K. Huebscher, A. Goschin, C. R. Smulski, E. Trompouki,
938 R. Link, H. Ebersbach, H. Srinivas, M. Marchant, G. Sogkas, D. Staab, C. Vågbø, D. Guerini, S.
939 Baasch, E. Latz, G. Hartmann, P. Henneke, R. Geiger, X. P. Peng, B. Grimbacher, E. Bartok, I.
940 Alseth, M. Warncke, M. Proietti, ADA2 is a lysosomal deoxyadenosine deaminase acting on DNA
941 involved in regulating TLR9-mediated immune sensing of DNA. *Cell Rep.* **43** (2024),
942 doi:10.1016/j.celrep.2024.114899.

943 29. H. Jee, Z. Huang, S. Baxter, Y. Huang, M. L. Taylor, L. A. Henderson, S. Rosenzweig, A. Sharma,
944 E. P. Chambers, M. S. Hershfield, Q. Zhou, F. Dedeoglu, I. Aksentijevich, P. A. Nigrovic, A.
945 O'Donnell-Luria, P. Y. Lee, Comprehensive analysis of ADA2 genetic variants and estimation of
946 carrier frequency driven by a function-based approach. *J. Allergy Clin. Immunol.* (2021),
947 doi:10.1016/j.jaci.2021.04.034.
948 30. M. A. Daniels, K. A. Hogquist, S. C. Jameson, Sweet "n" sour: the impact of differential
949 glycosylation on T cell responses. *Nat. Immunol.* **3**, 903–910 (2002).
950 31. S. Davidson, C.-H. Yu, A. Steiner, F. Ebstein, P. J. Baker, V. Jarur-Chamy, K. Hrovat Schaale, P.
951 Laohamonthonkul, K. Kong, D. J. Calleja, C. R. Harapas, K. R. Balka, J. Mitchell, J. T. Jackson,
952 N. D. Geoghegan, F. Moghaddas, K. L. Rogers, K. D. Mayer-Barber, A. A. De Jesus, D. De Nardo,
953 B. T. Kile, A. J. Sadler, M. C. Poli, E. Krüger, R. Goldbach Mansky, S. L. Masters, Protein kinase
954 R is an innate immune sensor of proteotoxic stress via accumulation of cytoplasmic IL-24. *Sci.*
955 *Immunol.* **7**, eabi6763 (2022).
956 32. L. Dong, W. Luo, S. Maksym, S. C. Robson, A. V. Zavialov, Adenosine deaminase 2 regulates the
957 activation of the toll-like receptor 9 in response to nucleic acids. *Front. Med.* (2024),
958 doi:10.1007/s11684-024-1067-5.
959 33. M.-S. Kim, D. Leahy, in *Methods in Enzymology*, Laboratory Methods in Enzymology: Cell, Lipid
960 and Carbohydrate. J. Lorsch, Ed. (Academic Press, 2013), vol. 533, pp. 259–263.
961 34. N. Watanabe, S. Gao, Z. Wu, S. Batchu, S. Kajigaya, C. Diamond, L. Alemu, D. Q. Raffo, P.
962 Hoffmann, D. Stone, A. K. Ombrello, N. S. Young, Analysis of deficiency of adenosine deaminase
963 2 pathogenesis based on single-cell RNA sequencing of monocytes. *J. Leukoc. Biol.* **110**, 409–424
964 (2021).
965 35. K. Pakos-Zebrucka, I. Koryga, K. Mnich, M. Ljujic, A. Samali, A. M. Gorman, The integrated
966 stress response. *EMBO Rep.* **17**, 1374–1395 (2016).

967 36. S. Cooray, E. Omyinmi, Y. Hong, C. Papadopoulou, L. Harper, E. Al-Abadi, R. Goel, S. Dubey,
968 M. Wood, S. Jolles, S. Berg, M. Ekelund, K. Armon, D. Eleftheriou, P. A. Brogan, Anti-tumour
969 necrosis factor treatment for the prevention of ischaemic events in patients with deficiency of
970 adenosine deaminase 2 (DADA2). *Rheumatol. Oxf. Engl.* **60**, 4373–4378 (2021).
971 37. P. Y. Lee, B. A. Davidson, R. S. Abraham, B. Alter, J. I. Arostegui, K. Bell, A. Belot, J. R. E.
972 Bergerson, T. J. Bernard, P. A. Brogan, Y. Berkun, N. T. Deuitch, D. Dimitrova, S. A. Georgin-
973 Lavialle, M. Gattorno, B. Grimbacher, H. Hashem, M. S. Hershfield, R. N. Ichord, K. Izawa, J. A.
974 Kanakry, R. P. Khubchandani, F. C. C. Klouwer, E. A. Luton, A. W. Man, I. Meyts, J. M. Van
975 Montfrans, S. Ozen, J. Saarela, G. C. Santo, A. Sharma, A. Soldatos, R. Sparks, T. R. Torgerson, I.
976 L. Uriarte, T. A. B. Youngstein, Q. Zhou, I. Aksentijevich, D. L. Kastner, E. P. Chambers, A. K.
977 Ombrello, DADA2 Foundation, Evaluation and Management of Deficiency of Adenosine
978 Deaminase 2: An International Consensus Statement. *JAMA Netw. Open* **6**, e2315894 (2023).
979 38. J. G. Doench, N. Fusi, M. Sullender, M. Hegde, E. W. Vaimberg, K. F. Donovan, I. Smith, Z.
980 Tothova, C. Wilen, R. Orchard, H. W. Virgin, J. Listgarten, D. E. Root, Optimized sgRNA design
981 to maximize activity and minimize off-target effects of CRISPR-Cas9. *Nat. Biotechnol.* **34**, 184–191
982 (2016).
983 39. J. Rappsilber, Y. Ishihama, M. Mann, Stop and go extraction tips for matrix-assisted laser
984 desorption/ionization, nanoelectrospray, and LC/MS sample pretreatment in proteomics. *Anal.*
985 *Chem.* **75**, 663–670 (2003).
986 40. S. Tyanova, T. Temu, J. Cox, The MaxQuant computational platform for mass spectrometry-based
987 shotgun proteomics. *Nat Protoc* **11**, 2301–2319 (2016).
988 41. J. Illingworth, Methods of enzymatic analysis: Third edition: Editor-in-Chief: Hans Ulrich
989 Bergmeyer. Verlag Chemie, 1983 (vols I–III), 1984 (vols IV & V) DM258 each volume or DM2240
990 vols I–X inclusive. *Biochem. Educ.* **13**, 38–38 (1985).

991 42. K. J. Livak, T. D. Schmittgen, Analysis of relative gene expression data using real-time quantitative
992 PCR and the 2(-Delta Delta C(T)) Method. *Methods San Diego Calif* **25**, 402–408 (2001).
993 43. S. Tyanova, T. Temu, P. Sinitcyn, A. Carlson, M. Y. Hein, T. Geiger, M. Mann, J. Cox, The Perseus
994 computational platform for comprehensive analysis of (prote)omics data. *Nat. Methods* **13**, 731–740
995 (2016).
996 44. A. Sharma, G. Naidu, V. Sharma, S. Jha, A. Dhooria, V. Dhir, P. Bhatia, V. Sharma, S. Bhattad, K.
997 G. Chengappa, V. Gupta, D. P. Misra, P. P. Chavan, S. Malaviya, R. Dudam, B. Sharma, S. Kumar,
998 R. Bhojwani, P. Gupta, V. Agarwal, K. Sharma, M. Singhal, M. Rathi, R. Nada, R. W. Minz, V.
999 Chaturvedi, A. Aggarwal, R. Handa, A. Grossi, M. Gattorno, Z. Huang, J. Wang, R. Jois, V. S.
1000 Negi, R. Khubchandani, S. Jain, J. I. Arostegui, E. P. Chambers, M. S. Hershfield, I. Aksentijevich,
1001 Q. Zhou, P. Y. Lee, Deficiency of Adenosine Deaminase 2 in Adults and Children: Experience
1002 From India. *Arthritis Rheumatol. Hoboken NJ* **73**, 276–285 (2021).
1003 45. R. Caorsi, F. Penco, A. Grossi, A. Insalaco, A. Omenetti, M. Alessio, G. Conti, F. Marchetti, P.
1004 Picco, A. Tommasini, S. Martino, C. Malattia, R. Gallizzi, R. A. Podda, A. Salis, F. Falcini, F.
1005 Schena, F. Garbarino, A. Morreale, M. Pardeo, C. Ventrici, C. Passarelli, Q. Zhou, M. Severino, C.
1006 Gandolfo, G. Damonte, A. Martini, A. Ravelli, I. Aksentijevich, I. Ceccherini, M. Gattorno, ADA2
1007 deficiency (DADA2) as an unrecognised cause of early onset polyarteritis nodosa and stroke: a
1008 multicentre national study. *Ann. Rheum. Dis.* **76**, 1648–1656 (2017).
1009 46. J. Schepp, M. Proietti, N. Frede, M. Buchta, K. Hübscher, J. Rojas Restrepo, S. Goldacker, K.
1010 Warnatz, J. Pachlopnik Schmid, A. Duppenthaler, V. Lougaris, I. Uriarte, S. Kelly, M. Hershfield,
1011 B. Grimbacher, Screening of 181 Patients With Antibody Deficiency for Deficiency of Adenosine
1012 Deaminase 2 Sheds New Light on the Disease in Adulthood. *Arthritis Rheumatol. Hoboken NJ* **69**,
1013 1689–1700 (2017).

47. S. Özen, E. D. Batu, E. Z. Taşkıran, H. A. Özkara, Ş. Ünal, N. Güleray, A. Erden, Ö. Karadağ, F. Gümrük, M. Çetin, H. E. Sönmez, Y. Bilginer, D. Ç. Ayvaz, I. Tezcan, A Monogenic Disease with a Variety of Phenotypes: Deficiency of Adenosine Deaminase 2. *J. Rheumatol.* **47**, 117–125 (2020).
48. A. Betrains, F. Staels, L. Moens, S. Delafontaine, M. S. Hershfield, D. Blockmans, A. Liston, S. Humblet-Baron, I. Meyts, R. Schrijvers, S. Vanderschueren, Diagnosis of deficiency of adenosine deaminase type 2 in adulthood. *Scand. J. Rheumatol.* , 1–4 (2021).
49. O. Akgun-Dogan, P. O. Simsek-Kiper, E. Taskiran, C. Lissewski, J. Brinkmann, D. Schanze, R. Göçmen, D. Cagdas, Y. Bilginer, G. E. Utine, M. Zenker, S. Ozen, İ. Tezcan, M. Alikasifoglu, K. Boduroğlu, ADA2 deficiency in a patient with Noonan syndrome-like disorder with loose anagen hair: The co-occurrence of two rare syndromes. *Am. J. Med. Genet. A.* **179**, 2474–2480 (2019).
50. M. Rama, C. Duflos, I. Melki, D. Bessis, A. Bonhomme, H. Martin, D. Doummar, S. Valence, D. Rodriguez, E. Carme, D. Genevieve, K. Heimdal, A. Insalaco, N. Franck, V. Queyrel-Moranne, N. Tieulie, J. London, F. Uettwiller, S. Georgin-Lavialle, A. Belot, I. Koné-Paut, V. Hentgen, G. Boursier, I. Touitou, G. Sarrabay, A decision tree for the genetic diagnosis of deficiency of adenosine deaminase 2 (DADA2): a French reference centres experience. *Eur. J. Hum. Genet. EJHG* **26**, 960–971 (2018).
51. A. K. Ombrello, J. Qin, P. M. Hoffmann, P. Kumar, D. Stone, A. Jones, T. Romeo, B. Barham, G. Pinto-Patarroyo, C. Toro, A. Soldatos, Q. Zhou, N. Deuitch, I. Aksentijevich, S. L. Sheldon, S. Kelly, A. Man, K. Barron, M. Hershfield, W. A. Flegel, D. L. Kastner, Treatment Strategies for Deficiency of Adenosine Deaminase 2. *N. Engl. J. Med.* **380**, 1582–1584 (2019).
52. K. M. Gibson, K. A. Morishita, P. Dancey, P. Moorehead, B. Drögemöller, X. Han, J. Graham, R. E. W. Hancock, D. Foell, S. Benseler, R. Luqmani, R. S. M. Yeung, S. Shenoi, M. Bohm, A. M. Rosenberg, C. J. Ross, D. A. Cabral, K. L. Brown, Identification of Novel Adenosine Deaminase

1037 2 Gene Variants and Varied Clinical Phenotype in Pediatric Vasculitis. *Arthritis Rheumatol. Hoboken*
1038 *NJ* **71**, 1747–1755 (2019).

1039

1040 Abbreviations

1041	ADA2	Adenosine deaminase 2
1042	BFA	Brefeldin A
1043	DADA2	Deficiency of adenosine deaminase 2
1044	Endo H	Endoglycosidase H
1045	ER	Endoplasmic reticulum
1046	GM-CSF	Granulocyte–macrophage colony-stimulating factor
1047	HC	Healthy control
1048	HMDM	Human monocyte-derived macrophages
1049	HMW	High-molecular-weight
1050	LMW	Low-molecular-weight
1051	M-CSF	Macrophage colony-stimulating factor
1052	PNGase F	Peptide-N-Glycosidase F
1053	TNFi	TNF inhibitors
1054	WT	Wild type

1055

1056 Acknowledgments

1057 We thank Prof. Jaak Jaeken, Prof. Daisy Rymen and Dr. Eva Morava-Kozicz for kindly sharing their
1058 expertise and insight on protein glycosylation. We thank Lotte Bral for her assistance in the production
1059 of the knock-out cell lines. Above all, we would like to express our gratitude to our patients and their

parents for their willingness to participate in our study and to their treating physicians and nurses for their efforts in the collection of research samples. The figures Fig. 2A, Fig. 3G, Fig. 5C, Fig. 6E, Fig. 7E, Fig. 8A and Fig. S8A were created with BioRender.com.

Funding

This project has received funding from the following sources:

European Research Council (ERC) under the European Union's Horizon 2020 research and innovation program GA No. 948959 (MORE2ADA2) (LE, MW, BP, MD, IM)

KU Leuven C1 Grant C16/18/007 (IM)

Research Foundation-Flanders (FWO) grant G0B5120N (IM)

Jeffrey Modell Foundation (IM)

ERN-RITA (IM)

Research Foundation – Flanders (FWO) grant 11E0123N (LE)

Charité – Universitätsmedizin Berlin and the Berlin Institute of Health BIH Charité Junior Clinician Scientist Fellowship (LE)

Research Foundation – Flanders (FWO) grant 11F4421N (SD)

Research Foundation – Flanders (FWO) grant 1805523N (RS)

Research Foundation – Flanders (FWO) grant G0A3320N (PA)

KU Leuven C14/21/095 InterAction consortium (PA)

EOS MetaNiche consortium N° 40007532 (PA)

iBOF/21/053 ATLANTIS network (PA)

EOS DECODE consortium N° 30837538 (PA)

1083 ## Author contributions

1084 Conceptualization and design: LE, LM, IM

1085 Material preparation and data collection: LE, AH, MW, BP, SD, MD, EFR, AD, JN, MK, LM

1086 Data analysis: LE, AH, MB, MK, LM

1087 Generation of ADA2 knock-out cell lines: LE, MJ, DD

1088 Proteomics analyses: MK, PM, MFM, TM

1089 Design of trafficking experiments: LE, LM, IM, FE

1090 Design of ER stress experiments: LE; LM, IM, PA

1091 Collection of clinical data and patient materials: LE, SD, GB, LDS, RS, SV, DC, IM

1092 Supervision: IM

1093 Writing – original draft: LE

1094 Writing – review & editing: all authors

1095

1096 ## Competing interests

1097 IM receives research funding from CSL-Behring outside this project. Other grant support was received
1098 from Octapharma, as well as Advisory Board honoraries from Takeda and Boehringer-Ingelheim -
1099 paid to the institution and outside the submitted work.

1100

1101 ## Data and materials availability

1102 All data needed to evaluate the conclusions of our study are provided in the manuscript or the
1103 Supplementary Materials. The mass spectrometry data have been deposited to the ProteomeXchange
1104 Consortium via the PRIDE partner repository with the dataset identifier PXD046128. The authors
1105 provide a supplementary file containing the original blots of all the presented data.

Figures

Figure 1

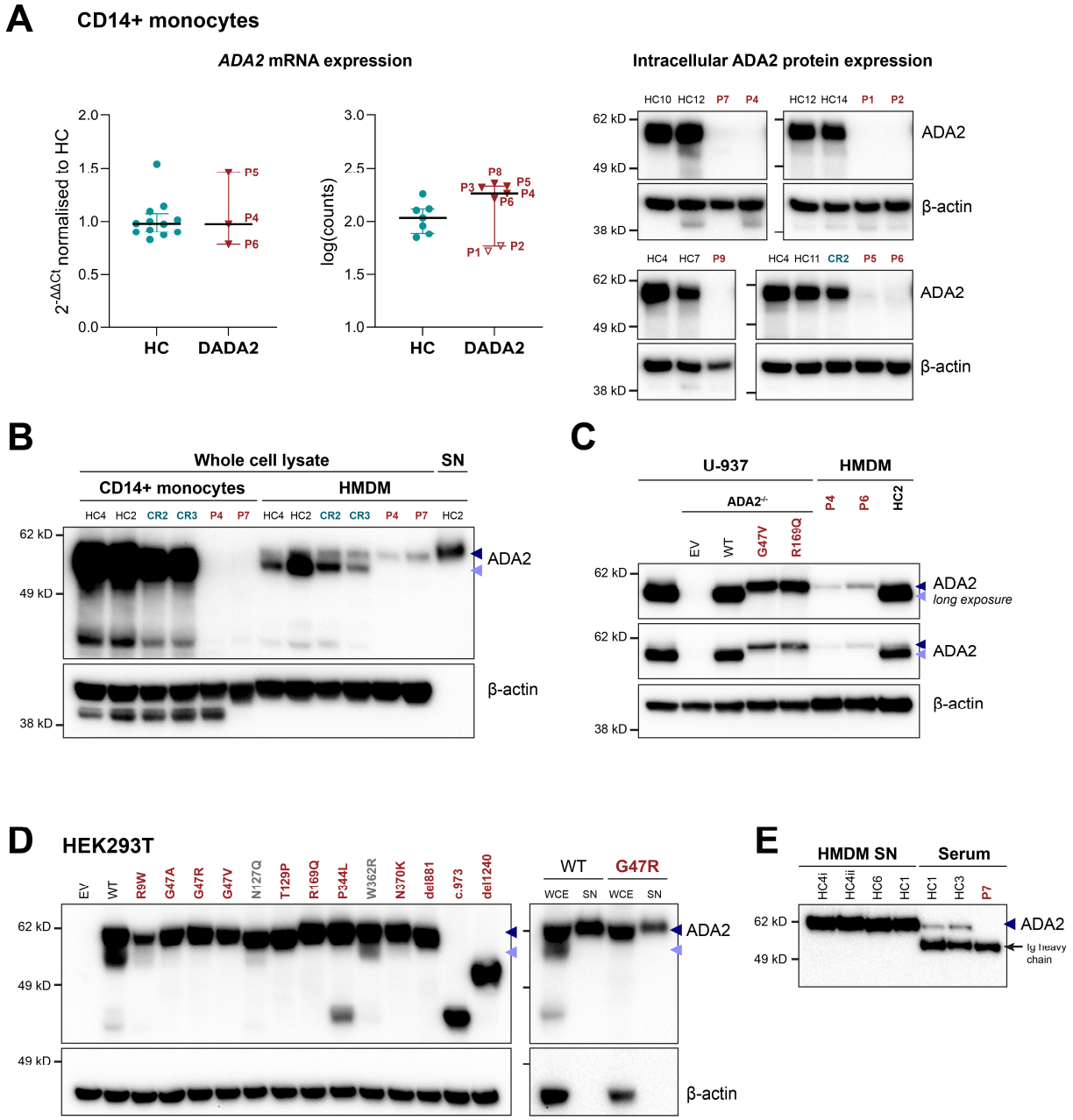

Fig. 1: Expression of pathogenic ADA2 protein variants. (A) mRNA and intracellular protein expression of *ADA2* in CD14^{+} monocytes from healthy controls (HC) and DADA2 patients (P) by qPCR or bulk RNA-sequencing and western blot of whole cell lysates, respectively. The left plot shows

1112 mRNA expression determined by qPCR. *ADA2* mRNA expression was normalized to *GAPDH* and
1113 is depicted relative to the mean of HC samples. The right plot shows counts determined by RNA-
1114 sequencing. Dot plots show median and interquartile range. **(B)** ADA2 protein expression in whole
1115 cell lysates and supernatant (SN) of $CD14^+$ monocytes and GM-CSF differentiated human monocyte-
1116 derived macrophages (HMDM) from HC, carriers (CR) and DADA2 patients (P) was determined by
1117 western blot. **(C)** ADA2 protein expression in whole cell lysates of transduced U-937 cells and HMDM
1118 from HC and DADA2 patients (P) was determined by western blot. **(D)** ADA2 protein expression in
1119 whole cell lysates of HEK293T cells after transfection with wild-type ADA2 and different pathogenic
1120 variants (*left*) and comparing whole cell lysates (WCE) and supernatant (SN) by western blot (*right*). **(E)**
1121 ADA2 protein expression in supernatants (SN) from healthy control human monocyte-derived
1122 macrophages (HMDM) and serum samples from healthy controls (HC) and DADA2 patients (P) by
1123 western blot using VeriBlot for detection. ADA2 detection using anti-ADA2 antibody clone
1124 EPR25430-131 (#ab288296; abcam) in all depicted western blots. Triangles indicate HMW-ADA2
1125 (dark blue) and LMW-ADA2 (light blue). Legend: Ig, immunoglobulin; WT, wild type.
1126

1127 **Figure 2**

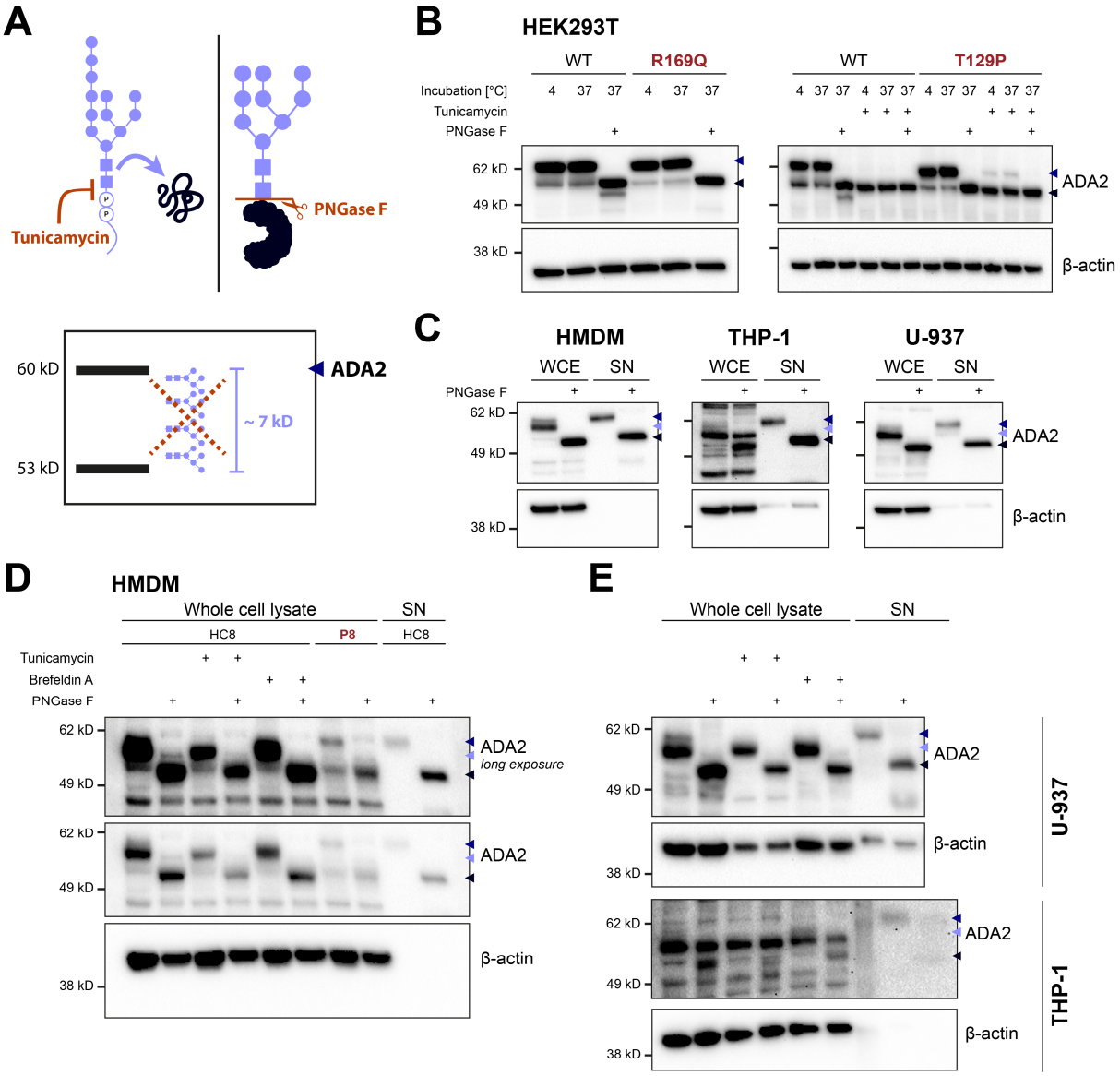

1128

1129 **Fig. 2: N-glycosylation of ADA2. (A)** Schematic illustration of inhibition of glycosylation by
1130 tunicamycin and glycan removal by PNGase F. **(B)** Western blot of wild-type (WT) ADA2 and the
1131 pathogenic variants p.R169Q and p.T129P transfected into HEK293T cells after incubation with or
1132 without 2.5 µg/mL tunicamycin for 24 h and/or glycan removal by PNGase F. **(C)** ADA2 protein
1133 expression by western blot in whole cell lysates (WCE) and supernatants (SN) of human monocyte-
1134 derived macrophages (HMDM), U-937 cells and THP-1 cells. **(D)** ADA2 protein expression in whole

1135 cell lysates and supernatants (SN) from GM-CSF-differentiated HMDM of healthy control HC8 and
1136 DADA2 patient P8 left untreated or treated with 5 μg/mL tunicamycin or 1 μg/mL brefeldin A for
1137 24 h. **(E)** ADA2 protein expression in whole cell lysates and supernatants (SN) from U-937 and THP-
1138 1 cells left untreated or treated with 2.5 μg/mL tunicamycin or 1 μg/mL brefeldin A for 24 h. Glycan
1139 removal was performed by incubation with PNGase F for 1 hour at 37°C under denaturing conditions
1140 in all experiments. ADA2 detection using anti-ADA2 (#HPA007888, Sigma-Aldrich) in all depicted
1141 western blots. Triangles indicate HMW-ADA2 (dark blue), LMW-ADA2 (light blue) and glycan-free
1142 ADA2 (black).
1143

1144 **Figure 3**

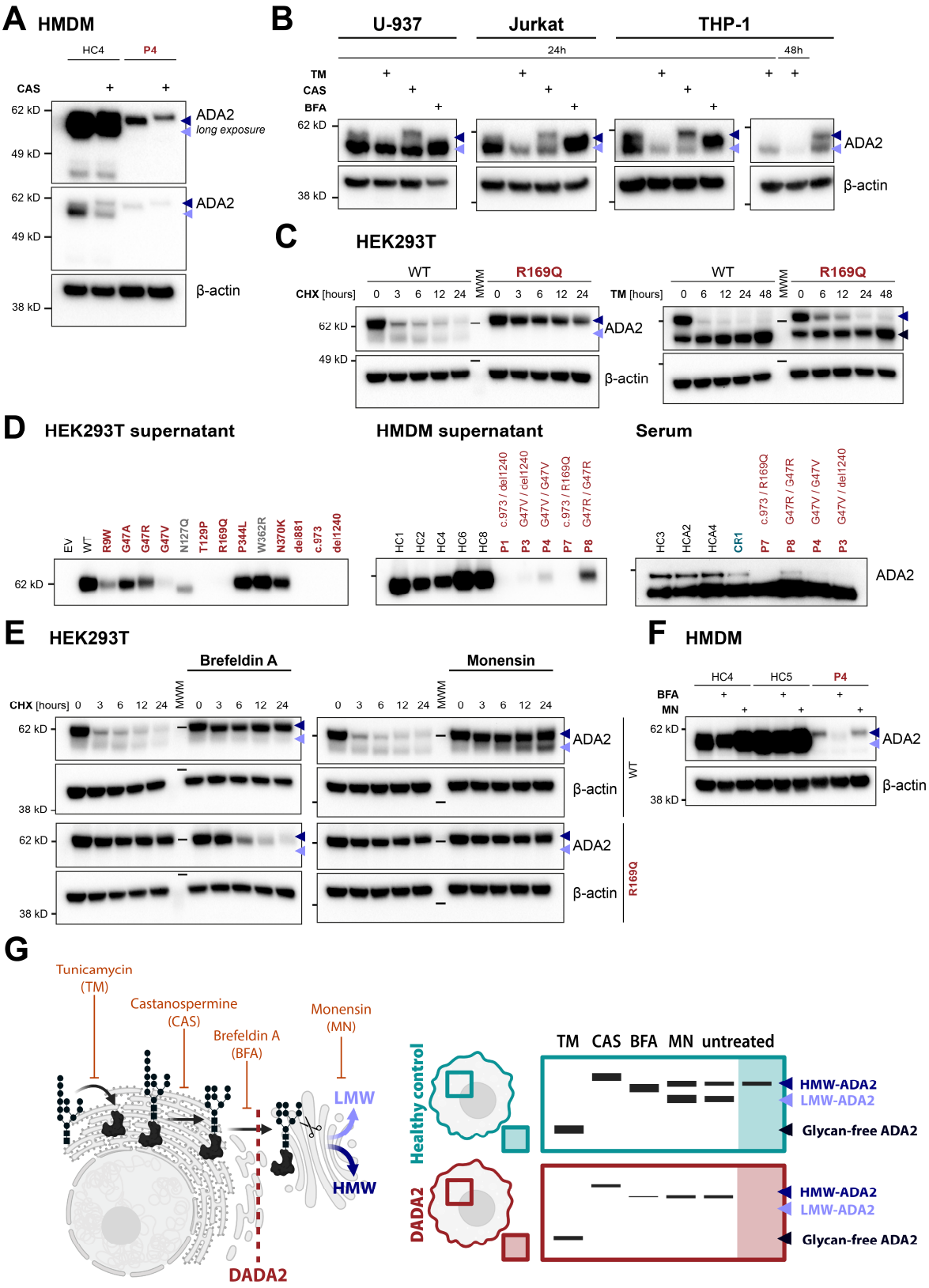

1145

1146 **Fig. 3: Glycan processing of ADA2 in the ER. (A)** ADA2 protein expression by western blot in
1147 GM-CSF-differentiated HMDM from healthy control HC4 and DADA2 patient P4 after incubation
1148 with 100 μg/mL castanospermine for 24 h. **(B)** ADA2 protein expression upon inhibition of N-
1149 glycosylation, ER glucosidases I and II, or ER to Golgi trafficking. U-937, THP-1 and Jurkat cells were
1150 incubated with 2.5 μg/mL tunicamycin (TM), 100 μg/mL castanospermine (CAS) or 1 μg/mL
1151 brefeldin A (BFA) for 24 h or 48 h. **(C)** HEK293T cells were transfected with wild-type (WT) ADA2
1152 or the pathogenic variant p.R169Q and treated with 500 μg/mL cycloheximide (CHX) or 2.5 μg/mL
1153 tunicamycin (TM) over 24-48 h. Whole cell lysates were generated at the indicated time points and
1154 immunoblotted for ADA2 expression. **(D)** ADA2 protein levels were determined in supernatants of
1155 M-CSF-differentiated human monocyte-derived macrophages (HMDM) from healthy controls (HC)
1156 or DADA2 patients (P) or HEK293T cells transfected with wild-type (WT) *ADA2* or different
1157 pathogenic *ADA2* variants. The patients' genotypes are indicated above. Western blot of serum
1158 samples from healthy controls (HC), heterozygous DADA2 carriers (CR) and DADA2 patients (P)
1159 detected by anti-ADA2 antibody clone EPR25430-131 (#ab288296; abcam) and VeriBlot.
1160 **(E)** HEK293T cells were transfected with wild-type (WT) ADA2 or different pathogenic variants and
1161 treated with 500 μg/mL cycloheximide (CHX) ± 1 μg/mL brefeldin A or 2 μg/mL monensin over
1162 24 h. Whole cell lysates were generated at the indicated time points and immunoblotted for ADA2
1163 expression. **(F)** ADA2 protein expression in GM-CSF-differentiated human monocyte-derived
1164 macrophages from healthy controls (HC) or DADA2 patient P4 left untreated or treated with 1 μg/mL
1165 brefeldin A (BFA) or 2 μg/mL monensin (MN). **(G)** Schematic overview of trafficking and processing
1166 of ADA2 in healthy control and DADA2 cells. ADA2 detection using anti-ADA2 antibody clone
1167 EPR25430-131 (#ab288296; abcam) in panels A, B, C (*left*), D, E and F and using anti-ADA2
1168 (#HPA007888, Sigma-Aldrich) in panel C (*right*). Triangles indicate HMW-ADA2 (dark blue), LMW-

1169 ADA2 (light blue) and glycan-free ADA2 (black). Legend: BFA, brefeldin A, CAS, castanospermine,

1170 EV, empty vector; MN, monensin, MWM, molecular weight marker; TM, tunicamycin; WT, wild type.

1171

1172 **Figure 4**

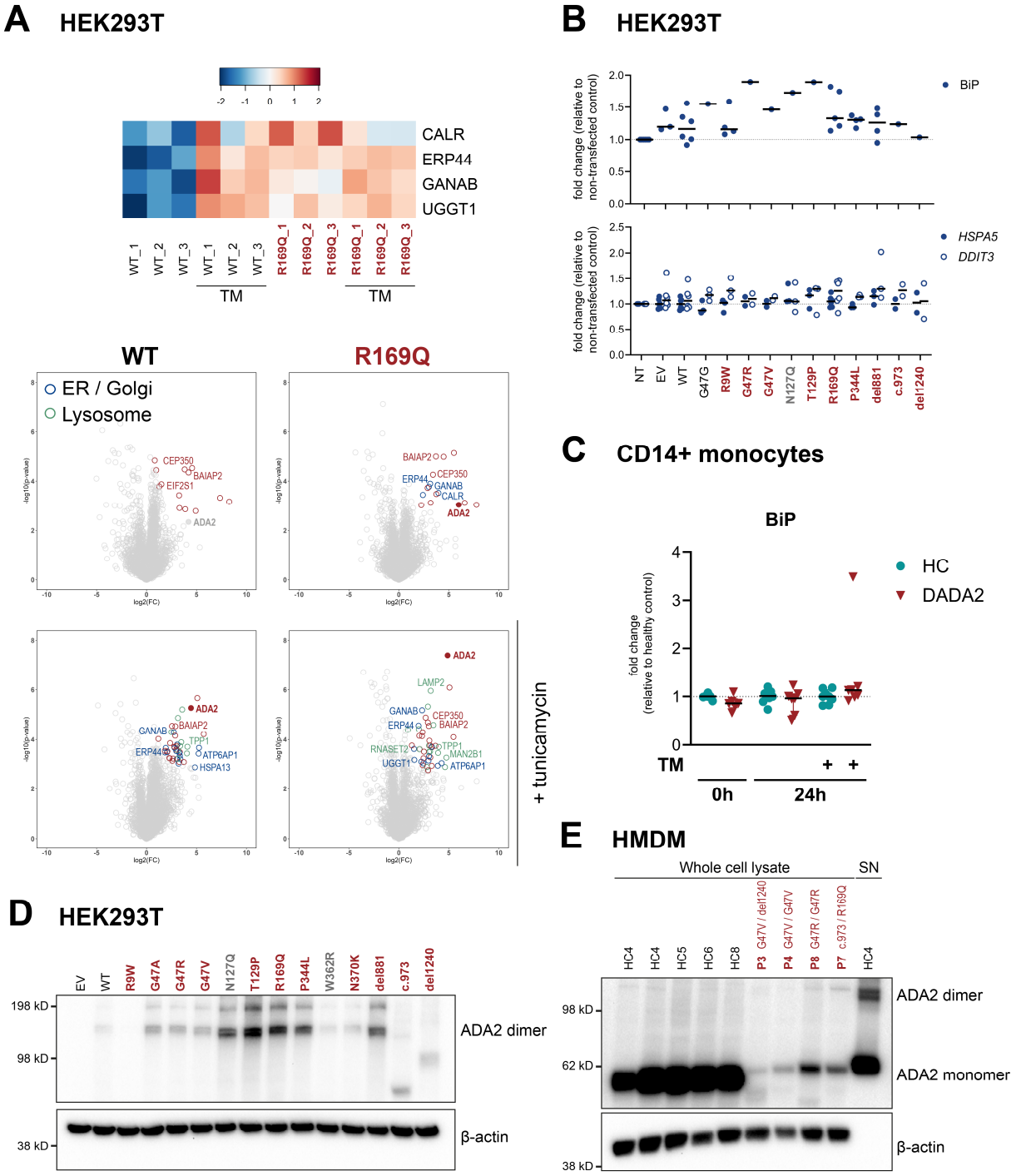

1173

1174 **Fig. 4: ER stress in DADA2. (A)** Interactome analysis of wild-type (WT) ADA2 and the pathogenic

1175 variant p.R169Q overexpressed in HEK293T cells treated with or without 2.5 µg/mL tunicamycin

1176 (TM) for 24 h was performed by immunoprecipitation followed by mass spectrometry. Heatmap
1177 shows z-score of protein abundance. Binders significantly pulled down compared to isotype control
1178 with a false discovery rate of 5% are highlighted by colored circles. Localization of the interacting
1179 proteins to the ER/Golgi (blue) or lysosome (green) is indicated by color. **(B)** ER stress response in
1180 HEK293T cells transfected with wild-type (WT) *ADA2* and different pathogenic variants. Protein
1181 expression of BiP (*top*) and mRNA expression of *HSPA5* and *DDIT3* (*bottom*) were determined 48h
1182 after transfection. A representative western blot is shown in **Fig. S5F**. mRNA expression was
1183 normalized to *GAPDH* and is depicted as $2^{-\Delta\Delta Ct}$ relative to non-transfected control samples. Results
1184 from 6 independent experiments are shown. Dot plots show median. **(C)** ER stress response was
1185 evaluated by protein expression of BiP in whole cell lysates of $CD14^+$ monocytes at baseline or after
1186 24 h incubation with or without 1 μg/mL tunicamycin (TM). BiP expression was normalized to β-
1187 actin. Dot plots show median and interquartile range. The corresponding western blots are shown in
1188 **Fig. S6**. **(D)** Formation of intracellular ADA2 dimers in HEK293T cells transfected with wild-type
1189 (WT) ADA2 and different pathogenic *ADA2* variants. The blot is equivalent to the one shown in
1190 **Fig. 1D**. **(E)** ADA2 protein expression and intracellular dimer formation in GM-CSF differentiated
1191 human monocyte-derived macrophages from healthy controls (HC) and DADA2 patients (P). ADA2
1192 detection using anti-ADA2 antibody clone EPR25430-131 (#ab288296; abcam) in all depicted western
1193 blots. Legend: EV, empty vector; FC, fold change; NT, non-transfected; WT, wild type.
1194

1195 **Figure 5**

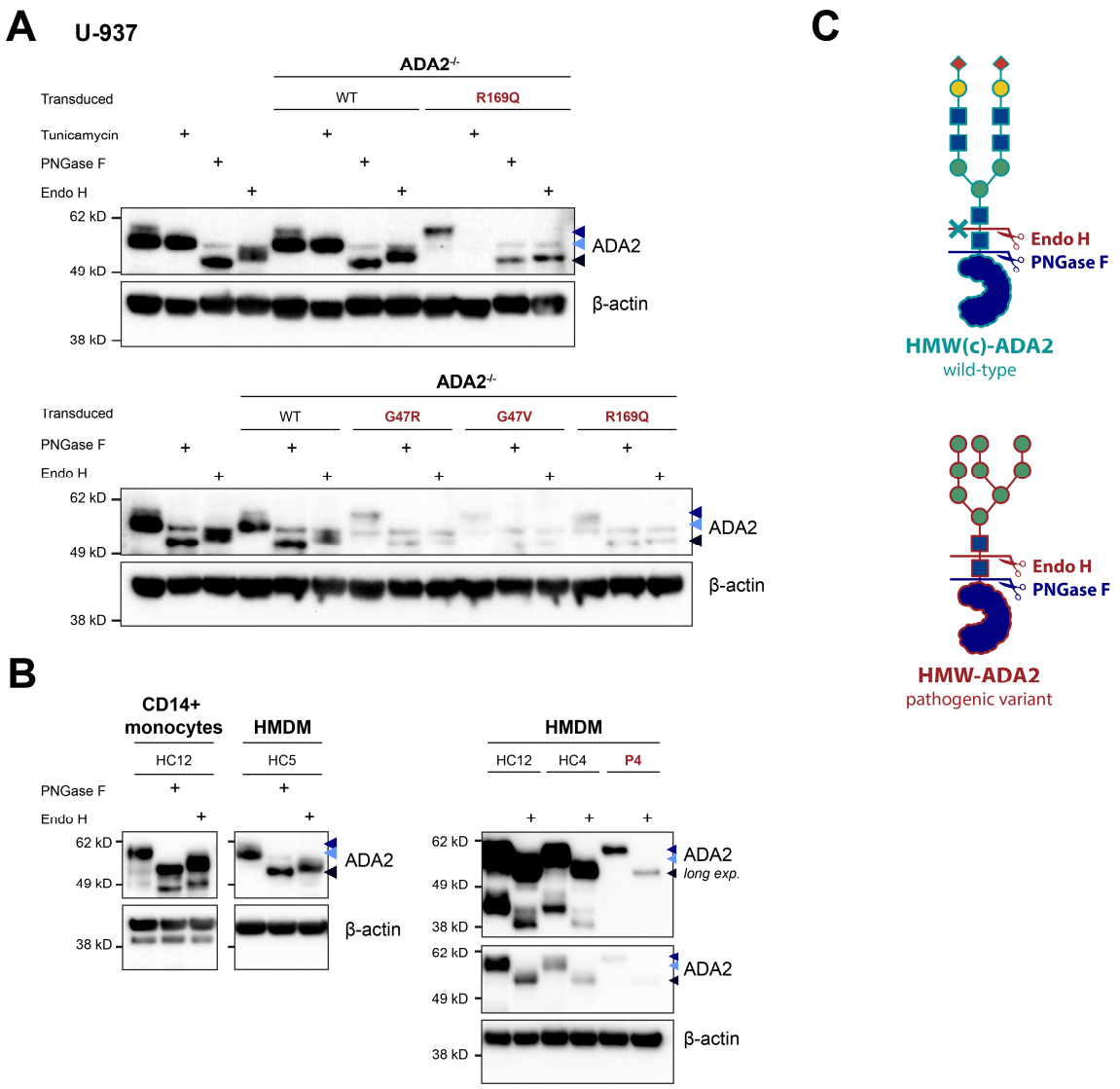

1196

1197 **Fig. 5: Glycan processing of HMW(c)-ADA2.** ADA2 protein expression by western blot after
1198 glycan removal in ADA2$^{WT/WT}$ and ADA2$^{-/-}$ U-937 cells transduced with pathogenic *ADA2* variants
1199 **(A)** and CD14^{+} monocytes or GM-CSF-differentiated HMDM from healthy controls (HC) and
1200 DADA2 patient P4 **(B)** by incubation with PNGase F or Endo H for 1 hour at 37 °C under denaturing
1201 conditions. **(C)** Cutting sites of PNGase F and Endo H. Endo H does not cleave complex glycans
1202 (*top*). Carbohydrate residues are depicted according to the Symbol Nomenclature for Glycans (SNFG)
1203 *(20)*. ADA2 detection using anti-ADA2 antibody clone EPR25430-131 (#ab288296; abcam) in panel

1204 B (*right*) and using anti-ADA2 (#HPA007888, Sigma-Aldrich) in panels A and B (*left*). Triangles indicate

1205 HMW-ADA2 (dark blue), LMW-ADA2 (light blue) and glycan-free ADA2 (black).

1206

1207 **Figure 6**

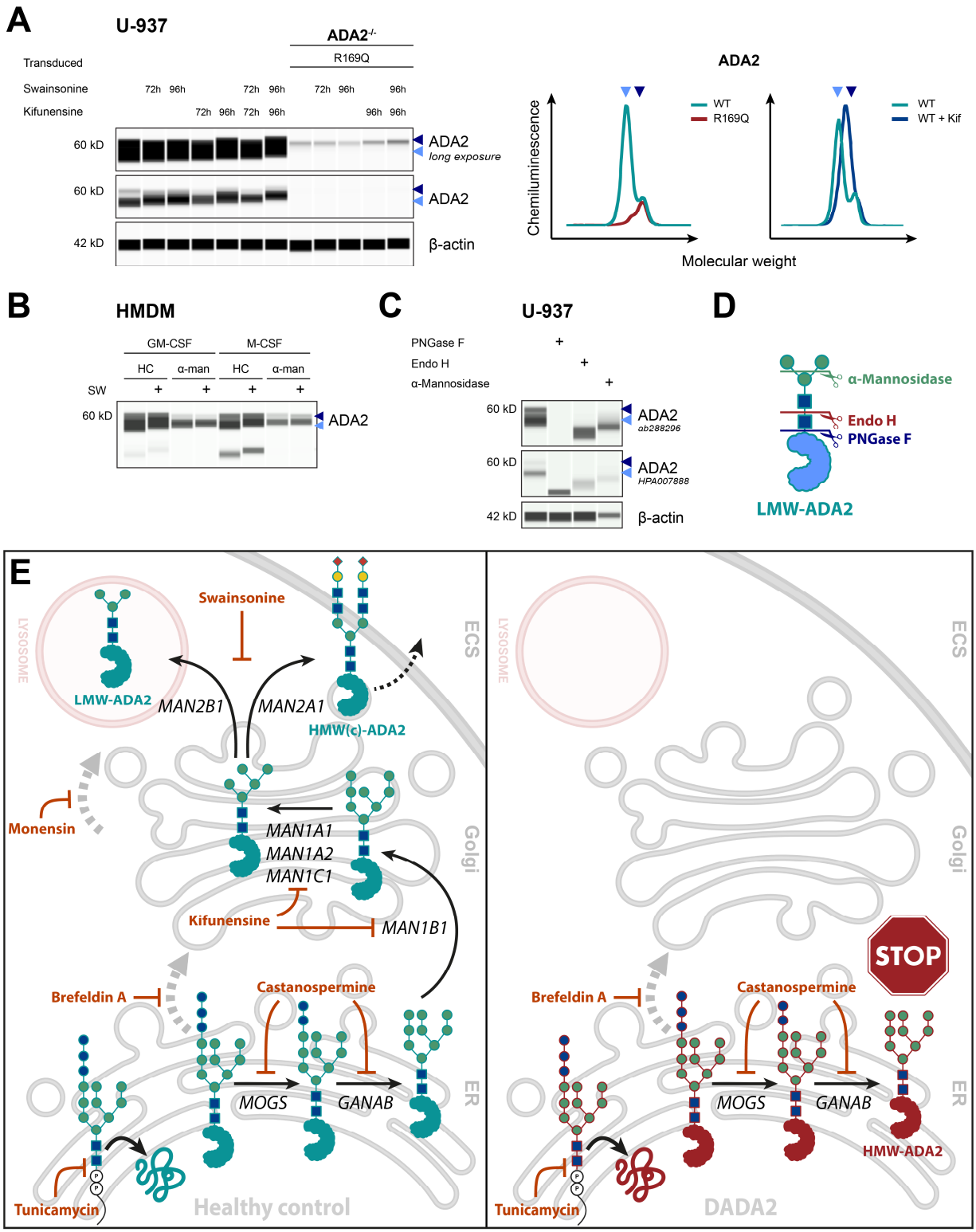

1208

1209 **Fig. 6: Glycan processing of LMW-ADA2. (A)** α-mannosidases were inhibited by 72-96 h
1210 incubation of $ADA2^{WT/WT}$ and $ADA2^{-/-}$ U-937 cells transduced with R169Q with 375 nM kifunensine
1211 and/or 10 μM swainsonine. ADA2 protein expression was determined by western blot. The
1212 histograms indicate molecular weight peaks as determined by Simple Western. The original graphs are
1213 provided in **Fig. S7**. **(B)** ADA2 protein expression by western blot GM-CSF- and M-CSF-
1214 differentiated HMDM from a healthy control (HC) and a patient with α-mannosidosis (α-man) after
1215 incubation with 10 μM swainsonine (SW) for 96 h. **(C)** ADA2 protein expression by western blot after
1216 glycan removal in $ADA2^{WT/WT}$ U-937 cells by incubation with PNGase F, Endo H or α1-2,3,6
1217 Mannosidase for 1 hour at 37 °C. **(D)** Cleavage sites of PNGase F, Endo H and α-Mannosidase. **(E)**
1218 Schematic overview of the trafficking and glycan modifications of ADA2 expressed in healthy control
1219 (*left*) and DADA2 (*right*) human monocyte-derived macrophages based on the findings presented in
1220 this article. *MOGS* encodes ER α-glucosidase I, *GANAB* encodes ER α-glucosidase II, *MAN1B1*
1221 encodes ER α-1,2-mannosidase, *MAN1A1*, *MAN1A2* and *MAN1C1* encode Golgi α-1,2-
1222 mannosidases, *MAN2A1* encodes Golgi α-mannosidase II, and *MAN2B1* encodes lysosomal α-
1223 mannosidase. Mechanisms of action of the inhibitors used for the *in vitro* study of glycan processing
1224 are depicted in orange. Carbohydrate residues are depicted according to the Symbol Nomenclature for
1225 Glycans (SNFG) *(20)*. ADA2 detection using anti-ADA2 antibody clone EPR25430-131 (#ab288296;
1226 abcam) in panels A, B and C (*top*) and using anti-ADA2 (#HPA007888, Sigma-Aldrich) in panel C
1227 (*bottom*). Triangles indicate HMW-ADA2 (dark blue), LMW-ADA2 (light blue) and glycan-free ADA2
1228 (black). Legend: ECS, extracellular space; ER, endoplasmic reticulum.
1229

1230 **Figure 7**

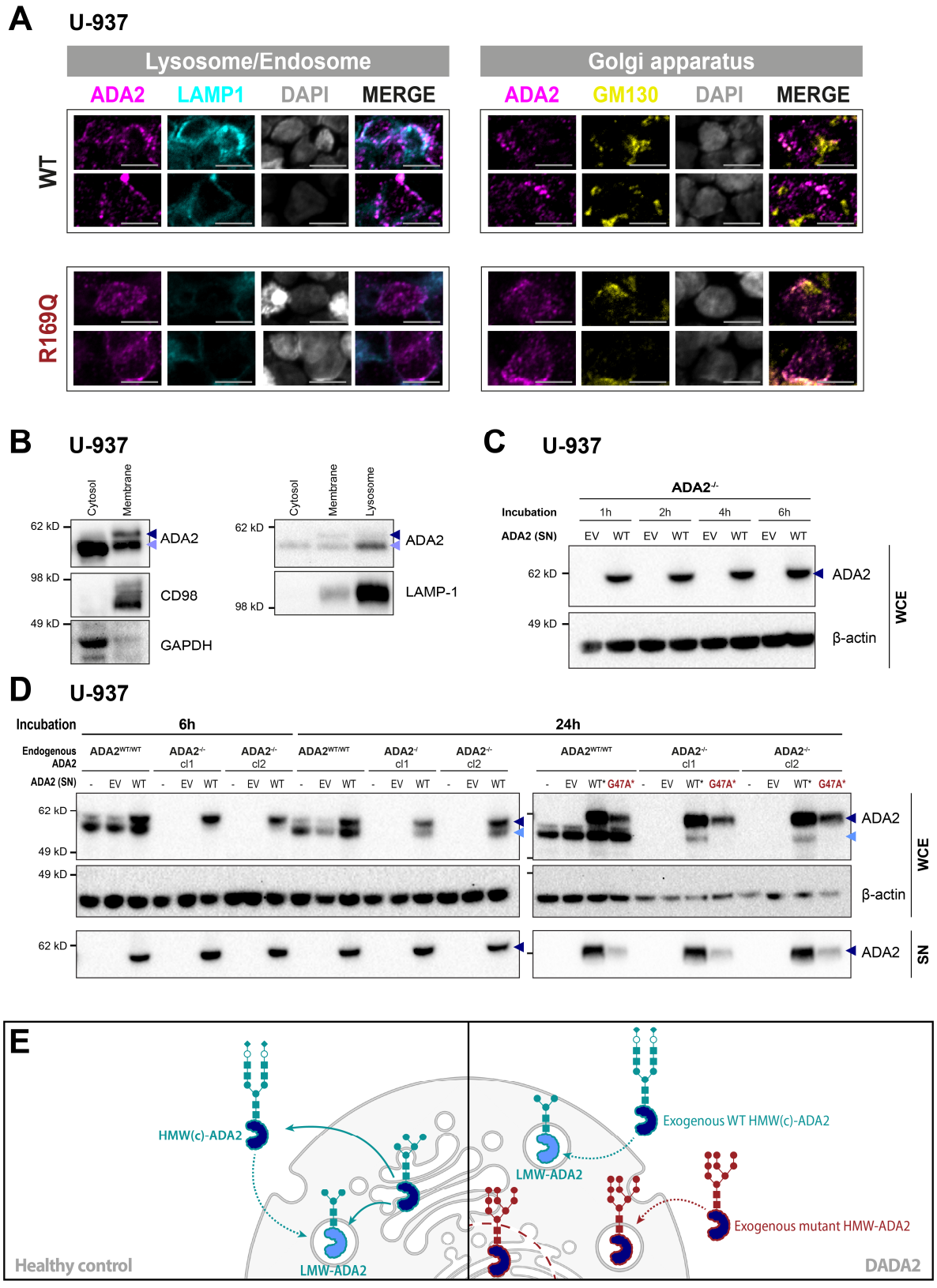

1231

1232 **Fig. 7: Localization and generation of LMW-ADA2. (A)** Immunofluorescence microscopy of
1233 $ADA2^{WT/WT}$ U-937 cells and $ADA2^{-/-}$ U-937 transduced with the pathogenic variant p.R169Q stained
1234 for ADA2 and markers of lysosomal (LAMP1) and Golgi (GM130) compartments. **(B)** ADA2 protein
1235 expression in cytosolic, membranous and lysosomal fractions of U-937 cells by western blot. **(C)**
1236 Intracellular ADA2 uptake into $ADA2^{-/-}$ U-937 cells after incubation with supernatants (SN) from
1237 HEK293T cells transfected with empty vector (EV) or wild-type (WT) *ADA2* for the indicated time.
1238 **(D)** Generation of intracellular LMW-ADA2 in $ADA2^{WT/WT}$ or $ADA2^{-/-}$ U-937 cells after incubation
1239 with supernatants (SN) from HEK293T cells transfected with empty vector (EV), wild-type (WT)
1240 *ADA2* or the pathogenic variant p.G47A for the indicated time. **(E)** Schematic illustration of uptake
1241 and processing of exogenous ADA2. ADA2 detection using anti-ADA2 antibody clone EPR25430-
1242 131 (#ab288296; abcam) in panels C and D and using anti-ADA2 (#HPA007888, Sigma-Aldrich) in
1243 panel B. Triangles indicate HMW-ADA2 (dark blue), LMW-ADA2 (light blue) and glycan-free ADA2
1244 (black). Legend: cl, clone.
1245

1246 **Figure 8**

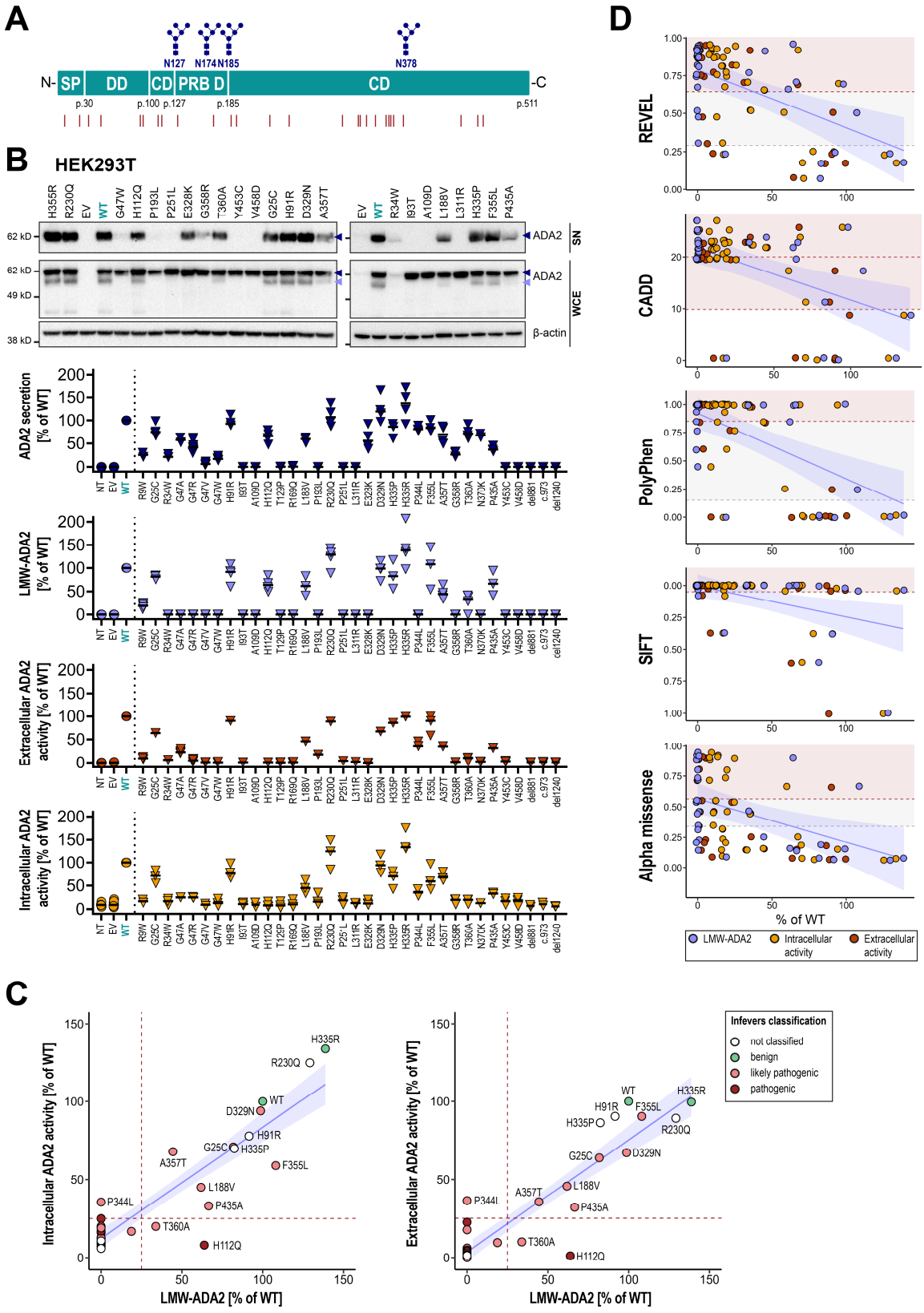

1247

1248 **Fig. 8: Validation of absent LMW-ADA2 as a pathogenicity marker of *ADA2* variants. (A)**
1249 Distribution of all evaluated ADA2 variants (red lines) across the ADA2 protein domains. The N-
1250 glycosylation sites are indicated in blue. **(B)** ADA2 secretion and LMW-ADA2 expression in
1251 HEK293T cells transfected with *ADA2* variants were determined by western blot using anti-ADA2
1252 antibody clone EPR25430-131 (#ab288296; abcam). Enzyme activity was measured in whole cell
1253 lysates and supernatants of the transfected cells. Dot plots show median. Each variant was examined
1254 in n=3-4 independent experiments. **(C)** Correlation of LMW-ADA2 and intracellular or extracellular
1255 ADA2 enzyme activity of *ADA2* variants expressed in HEK293T cells. The dots show median of
1256 n=3-4 independent experiments. The dotted lines indicate 25% expression/activity of WT ADA2. The
1257 blue line represents the fitted linear regression line with its 95% confidence interval shaded in light
1258 blue. **(D)** Correlation of LMW-ADA2 expression and ADA2 enzyme activity with different
1259 pathogenicity scores. Red shading indicates (likely) pathogenic scores while grey shading represents
1260 ambiguous scores. The blue line represents the fitted linear regression line with its 95% confidence
1261 interval shaded in light blue. The corresponding Pearson correlation coefficients are shown in Table
1262 S3. Legend: CD, catalytic domain; DD, dimerization domain; EV, empty vector; NT, non-transfected;
1263 PRB D, putative receptor binding domain; SP, signal peptide; WT, wild type.
1264

1265 # Tables

ID	Age [years]	Sex	Genotype	Predominant phenotype
P1	12	M	c.973-2A>G/c.del1240-1442; splice site (intron 6)/del exon 9	Vasculitis, hepatosplenomegaly, hypogammaglobulinemia
P2	14	F	c.973-2A>G/c.del1240-1442; splice site (intron 6)/del exon 9	Vasculitis, warts, arthralgia, hypo-gammaglobulinemia,
P3	26	M	c.140G>T/c.del1240-1442; p.G47V/del exon 9	Bone marrow failure, hypogam-maglobulinemia, hepatosplenomegaly
P4	26	M	c.140G>T/c.140G>T; p.G47V/p.G47V	Hypogammaglobulinemia, hepatosplenomegaly
P5	6	F	c.140G>T/c.506G>A; p.G47V/p.R169Q	Hypogammaglobulinemia, hepatosplenomegaly, stroke
P6	9	F	c.140G>T/c.506G>A; p.G47V/p.R169Q	Bone marrow failure, hypogam-maglobulinemia, hepatosplenomegaly
P7	32	F	c.973-2A>G/c.506G>A; splice site (intron 6)/p.R169Q	Stroke, hypertension
P8	16	M	c.139G>A/c.139G>A; p.G47R/p.G47R	Stroke, vasculitis

P9	10	F	c.973-2A>G/c.973-2A>G; splice site (intron 6)/splice site (intron 6)	Vasculitis, hypogammaglobulinemia
P10	50	F	c.973-2A>G/c.506G>A; splice site (intron 6)/p.R169Q	Vasculitis, leukopenia
CR1	39	F	WT/c. del1240-1442; WT/del exon 9	
CR2	38	F	WT/c.140G>T; WT/p.G47V	
CR3	42	M	WT/c.506G>A; WT/p.R169Q	

1266 **Table 1: Cohort characteristics.** Genotype and clinical phenotype of the included DADA2 patients

1267 (P) and heterozygous carriers (CR).

Protein	LMW-ADA2	ADA2 enzyme activity	REVEL	CADD	PolyPhen	SIFT	Alpha missense	Infevers	ClinVar	Homo-zygous patients	Hetero-zygous patients	Homozygous individuals in gnomAD
p.G25C	81.8	64.0	0.076	0.498	benign (0)	tolerated (0.61)	likely benign (0.0748)	likely pathogenic	uncertain significance	2	0	-
p.H91R	91.6	90.5	0.248	0.086	benign (0.001)	tolerated (0.38)	likely benign (0.0686)	not classified	uncertain significance	1	0	2
p.H112Q	63.9	**1.1**	**0.956**	**19.6**	**probably damaging (0.987)**	**deleterious (0)**	likely pathogenic (0.9015)	pathogenic	pathogenic/likely pathogenic	1	11	-
p.L188V	61.8	45.7	**0.657**	**21.8**	**possibly damaging (0.841)**	**deleterious (0)**	likely benign (0.1571)	likely pathogenic	conflicting	0	2	2
p.R230Q	129.2	89.3	0.232	0.437	benign (0.007)	tolerated (1)	likely benign (0.0611)	not classified	likely benign	0	0	2
p.D329N	98.7	67.3	**0.694**	**25.7**	**probably damaging (1)**	**deleterious (0.02)**	likely benign (0.1525)	likely pathogenic	uncertain significance	1	0	-

p.H335P	82.4	86.4	0.175	**11.27**	benign (0.012)	**deleterious (0)**	likely benign (0.1858)	not classified	uncertain significance	0	1	-
p.H335R	138.8	99.6	0.176	8.752	benign (0.015)	**deleterious (0.04)**	likely benign (0.0727)	benign	benign	0	0	94070
p.P344L	**0**	36.3	0.52	**22.3**	**probably damaging (0.979)**	**deleterious (0)**	ambiguous (0.4429)	likely pathogenic	NA	0	3	-
p.F355L	108.1	90.5	0.502	**17.34**	benign (0.25)	**deleterious (0.04)**	likely pathogenic (0.6625)	likely pathogenic	conflicting	0	2	-
p.A357T	44.5	35.5	**0.919**	**23.8**	**probably damaging (0.993)**	**deleterious (0)**	likely benign (0.2518)	likely pathogenic	conflicting	1	3	-
p.T360A	33.8	**10.0**	**0.774**	**22.8**	**probably damaging (0.994)**	**deleterious (0)**	ambiguous (0.465)	likely pathogenic	pathogenic	10	15	-
p.P435A	66.6	32.0	**0.706**	**22.8**	**probably damaging (0.997)**	**deleterious (0)**	likely benign (0.1426)	likely pathogenic	likely benign	0	2	-

1268 **Table 2: Variant characteristics.** Classification of *ADA2* variants exhibiting inconclusive (> 25% of WT) levels of LMW-ADA2 expression or ADA2

1269 enzyme activity. LMW-ADA2 expression and extracellular ADA2 enzyme activity are displayed as % of WT ADA2.